How meso shear chains bridge multiscale shear behaviors in granular materials: a preliminary study

Jiaying Liu, Antoine Wautier, François Nicot, F. Darve, Wei Zhou

How meso shear chains bridge multiscale shear behaviors in granular materials: a preliminary study

Jiaying Liu[a,b], Antoine Wautier[c], François Nicot[d,e], Félix Darve[f], Wei Zhou[g]

[a]*Department of Civil Engineering, Zhejiang University City College, Hangzhou 310015, China*
[b]*Zhejiang Engineering Research Center of Intelligent Urban Infrastructure, Hangzhou, 310015, China*
[c]*INRAE UR RECOVER, 3275 Rte Cézanne, CS 40061, 13182 Aix-en-Provence Cedex 5, France*
[d]*Université Grenoble Alpes, INRAE, UR ETGR, F-38402 St-Martin-d'Hères, France*
[e]*Laboratoire EDYTEM – USMB/CNRS, UMR 5204, Université Savoie Mont Blanc, Le Bourget-du-Lac 73376,France*
[f]*Université Grenoble Alpes, CNRS, G-INP, Laboratoire 3SR UMR5521, F-38000 Grenoble, France*
[g]*State Key Laboratory of Water Resources and Hydropower Engineering Science, Wuhan University, Wuhan 430072, China*

Abstract

The "incremental shear strain chain" concept (simply called "shear chain") has been proposed recently to quantitatively account for local kinematic features of granular materials. At the microscopic scale, contacts can slide and particles can rotate; while at the macroscopic scale, shear bands appear as a typical localized failure mode. Despite visual spatial distribution features, the direct links from microscopic to macroscopic shear behaviors are still missing. This paper investigates shear characteristics appearing at the micro, meso and macro scales in granular materials, and tries to elucidate how they can be correlated by adopting the shear chain concept. Based on the spatial statistics tools, the shear chain and the shear band orientations are compared by demonstrating that the shear band is influenced by the sample aspect ratio while shear chain orientation only depends on the stress state. Shear chains experience a relative steady and high fabric anisotropy, irrespective to the stress state. Micro contact sliding and particle rotation mainly exist in the shear chain connection positions, which gives possible clues on shear chain forming. In conclusion, the shear band is eventually conjectured to be formed of a collection of crossing shear chains at meso scale, according to detailed analysis and discussion on the correlations of shear behaviors across scales.

Keywords: granular materials, DEM, contact sliding, shear chain, shear band, particle rotation

Email addresses: liujy@zucc.edu.cn (Jiaying Liu), antoine.wautier@inrae.fr (Antoine Wautier), francois.nicot@inrae.fr (François Nicot), felix.darve@3sr-grenoble.fr (Félix Darve), zw_mxx@whu.edu.cn (Wei Zhou)

1. Introduction

For frictional granular materials, such as sands or coarse-grained soils, shear behaviors have been attracting much scientific attention for a long time. Indeed, the failure in geomaterials is closely related to the shear behavior, giving rise to mass-driven natural hazards [1, 2]. Under shearing loads, complex mechanical features are found in granular materials due to the disordered discrete structures and various components. The critical state [3, 4, 5], dilatancy [6, 7, 8], failure patterns [9, 10, 11] and many other phenomena are triggered by shearing but not well described in constitutive models, while multiscale investigations provide new clues for describing this constitutive complexity [12]. Shear banding, which relates to the macroscopic strain localization of a narrow band, is one of the typical failure patterns under shearing for granular materials. Although shear band orientation and width have been studied for a long time [13, 14], the intrinsic origin of this macroscopic strain localization still remains to be solved from the micro or meso scale explanations [15, 16, 17, 18, 19, 20]. Among the established results, the local meso slip structures have been observed within the granular assembly under shearing. They are suspected to play a major role in linking the local rearrangement and the macroscopic shear banding.

The granular micro-mechanics have been investigated from both numerical and experimental explorations during decades [21, 22, 23, 24], and then micromechanical models have been proposed [25, 26, 27, 28, 29]. Contacts between particles give rise to forces with or without the consideration of friction or cohesion, and the statistical characterization of forces and contact network finally result in the stress of the overall assembly. Microscopic features, such as particle size[30, 31, 32], particle shape [33, 34, 35] and particle breakage [36, 37, 38, 39], are also recognized to influence the macroscopic mechanical responses. For frictional granular materials, each contact is commonly assumed as elastoplastic, and the sliding is limited by the micro Coulomb friction at the contact scale. When one contact is sliding, i.e., two particles have relative tangential displacement, then it could be regarded as micro failure under shearing and related to local rearrangement [40]. Besides, at the microscopic scale, the rotation of particles will be triggered by the shear banding and concentrate within the localized area [41, 20, 42, 16]. So far, micromechanical ingredients like contact sliding and particle rotation have been involved in many researches on shear band forming, however, no direct links have been built to demonstrate that microscopic contact sliding or particle rotation trigger the macroscopic shear banding. Before shear band develops, the incremental deviatoric strain field already experiences a strain localization pattern but at a local scale, where sliding and rotation also reflect some spatial correlations to the incremental strain field [43]. It is therefore tempting to examine whether a bridge exists between microscopic shear behaviors and macroscopic shear banding.

Between the grain scale and the sample scale, there is an intermediate scale referred to as mesoscopic scale, where a few particles and relative voids form so-called mesostructures. For example, force chains and contact-based loops (or cycles, in 2D) are examples of such mesostructures. They have been defined to explore the force transmission and deformation mechanisms of granular materials under various loading conditions [44, 45, 46, 11]. Small localized patterns of the strain field before shear banding can be detected at the mesoscopic scale, which are called "microbands" in some publications [41, 47]. They have been analysed as meso-slip lines according to the solution of hyperbolic equations of plasticity theory [48]. In recent work of authors [49, 48], this mesoscopic shear structure has been defined as "incremental shear strain chain" (briefly "shear chain") by connecting cells with large deviatoric strain in the loop tessellation, which is inspired by force chain definition[44, 50]. The shear chain can well describe the orientated meso slip features, as well as the plasticity generation of granular materials during shearing. From a comprehensive comparisons of shear behaviors at micro, meso and macro scale, it should be meaningful to correlate the shear chain distribution and evolution to the contact sliding, grain rotation and shear banding. Once the link among the shear behaviors of the three scales is specified, a door will be opened to meticulously investigate the origin of shear banding.

Therefore in this paper, we try to identify the correlations from micro, meso to macroscopic shear behaviors at the primary stage. The Discrete Element Method (DEM) is used to perform the numerical tests, offering the advantage to obtain micro- and mesoscopic information inside granular assemblies. Section 2 briefly introduces shear behaviors at micro, meso and macro scales, particularly the shear chain structure which is defined in Liu et al. [49]. In Section 3, the spatial distribution patterns of incremental strains, particle rotations and contact sliding are compared for a typical biaxial test undergoing shear band formation. Then the orientation features of shear chain and shear band are compared in Section 4, demonstrating that they are different shear structures operating of different scales. The microscopic sliding and rotation have a preferred location in the shear chain connection positions, as investigated in Section 5. Combined with the results gained in this paper and conclusions in other publications (e.g., [43, 47]), the connecting role of meso shear chains between micro and macro shear behaviors is tried to be established in Section 6. The intermediate mesoscale shear strain chain is proved to be the key bridge from the micro to macro scales for granular materials under shearing.

2. Shear behaviors at micro, meso and macro scales

At the micro scale of granular materials, the basic elements, i.e., particles and contacts, are considered. By adopting the Coulomb friction criterion at micro scale, the contact sliding should be regarded as the shear behaviors at micro scale. As for a single particle, its rotation will be triggered by the tangential forces, then the particle rotation could be another sign of shearing at the micro scale.

When shearing loads are applied for granular materials, a number of mesoscopic slip structures will appear within the sample, which have been observed from numerical analysis and experimental tests [41, 47]. In Liu et al. [49], these meso slip structures have been defined as "incremental shear strain chains" (briefly "shear chains"), providing a way to describe the mesoscopic shear behaviors concretely. The shear chain, as shown in Figure 1, is captured by searching connecting meso loops [1] with large meso deviatoric strains by some assumptions. Here are the simplified steps for shear chain definition and obtaining[2]:

1. Compute the incremental strain tensor for each meso loop cell, then collect meso loops with incremental deviatoric strains larger than the average value (the given threshold).
2. Within the group of loops of larger incremental deviatoric strains, search loop chains by judging whether the deviation (β in Figure 1) between the maximum shearing directions of two connecting loops (dash-dotted line in Figure 1) and the geometric directions joining the 2 barycenters (black solid lines in Figure 1) are close. The connection between the two loops are built if β fulfills a given limitation, in this paper it is set as $\beta \leq \beta_{th} = 22.5°$. β_{th} denotes the threshold angle between these two directions.
3. If a chain of loops is composed of at least three loops, then it is regarded as a shear chain.

In Figure 1, there are key contacts and particles in forming a shear chain. The contact connecting two loops (red line in Figure 1) is called shear chain connection contact ("SCC" in Section 5.2), may exhibit significant features of sliding; the particles connected by shear chain

[1] polygons tessellated from the contact network, more details can be found in [51, 52]
[2] more details can be found in Liu et al. [49]

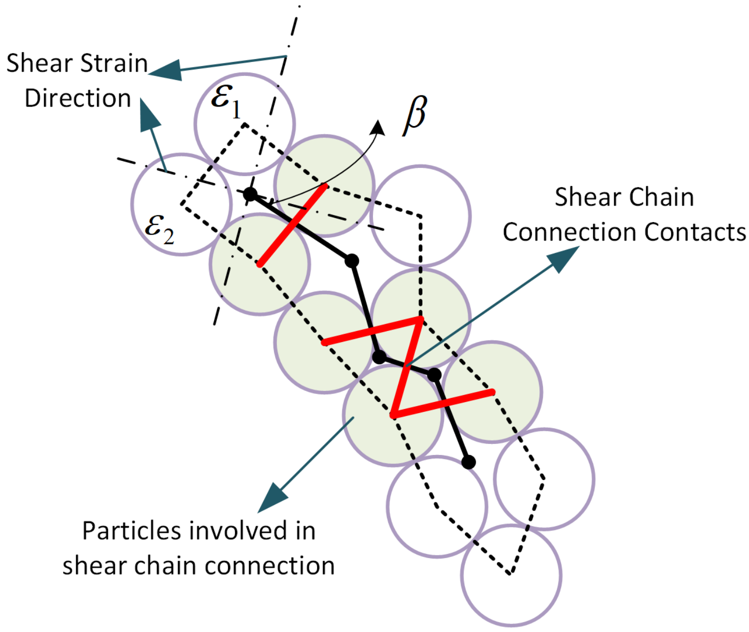

Figure 1: Schematic drawing of an incremental shear strain chain. β denotes the angle deviation between shear strain direction and the geometrical line connecting loop centers. Red lines are shear chain connection contacts, and their relative particles are marked in green.

contact (green sphere in Figure 1, "SC connex" in Section 5.3), could be imagined easier to rotate compared to other particles. In Section 5, these key micro matters will be carefully investigated.

The shear chain is a line-like structure, and we need to obtain its orientation angle θ. A representation of shear chains is achieved by joining the geometric barycenters of adjacent cells (dark thick line in Figure 1). For a shear chain of m adjacent mesoloops, the least square method defines the mean direction θ as:

$$\theta = \arctan\left(\frac{\sum_{i=1}^{m}(x_i - \bar{x})(y_i - \bar{y})}{\sum_{i=1}^{m}(x_i - \bar{x})^2}\right) \tag{1}$$

where x_i and y_i corresponds to the x and y coordinates of the geometric barycenter of loop cell i, and $\bar{x}$ and $\bar{y}$ are the averages of the x_i and y_i, respectively. Within a sheared granular assembly, there should be a number of shear chains. Then we choose the average absolute value of θ, i.e., $<|\theta|>$, to be an indicator for assessing the shear chain orientation of an assembly at a given state [49].

At the macro scale, shear bands are one of the typical failures for granular materials under shearing. The orientation and width of shear bands are usually focused on by researchers. Shear bands and shear chains are different but correlated somehow, which will be shown in Section 4 and 6.

3. Spatial distribution patterns during shear band forming

During deviatoric loading, dense granular materials usually experience a transition from a homogeneous to a heterogeneous kinematic pattern with respect to the commonly considered incremental deviatoric strain field. Besides, microscopic characterizations, such as particle rotation and contact sliding, demonstrate corresponding distribution features to the strain field. In this section, an example of biaxial drained test conducted by DEM is chosen, to show the visual features of shear band forming and the related microscopic features.

3.1. An example of DEM biaxial test

A series of biaxial tests are performed for dense assemblies by using the open-source DEM platform YADE [53]. Details of each DEM test are displayed in Appendix A. Here we select one of the samples, Sample DP[3], as an example to investigate the visual patterns of kinematic field. Initially, 33 333 spherical particles are generated within a rectangle of aspect ratio L/W=2.5, where L denotes the length and W denotes the width(the sketch of the sample is shown in Figure 2); then the rectangle sample is densely packed to reach an isotropic stress state of 100 kPa by the combining method of particle growing and boundary compaction[40]. After reaching the isotropic stress state, deviatoric loads are applied by compressing the upper and lower boundaries with the strain rate of $-0.01/s$ while keeping the lateral stress constant to 100 kPa. Rigid walls are used for sample boundaries. The uniform distribution is chosen with the ratio of the maximum diameter to the minimum $D_{max}/D_{min} = 1.98$ and the average size $D_{50} = 8.4$ mm. Other parameters in the DEM simulations: the material density is set to $\rho = 3,000$ kg.m^{-3}; k_n/D_s is set to 300 MPa, where $D_s = 2R_1R_2/(R_1 + R_2)$ and R_1, R_2 are the radii of particles in a given contact; k_t/k_n is set to 0.5. The information of other samples are shown in Appendix A, and the only difference between all 16 samples is the sample aspect ratio.

Figure 3 presents the curves of deviatoric stress and volumeteric strain evolutions along the biaxial drained test. Correspondingly, the incremental deviatoric and volumetric strain fields are shown in Figure 4 for five key states (A, B, C, D, E in Figure 3). The local strain is defined based on the contact loop tessellation. At the scale of a loop, incremental grain displacements are adopted to define an incremental strain tensor of the given loop. Detailed information of the

[3]We choose this sample because two bands form with different orientations at the final stage, which make convenience for analyzing the distribution features of micro characterizations

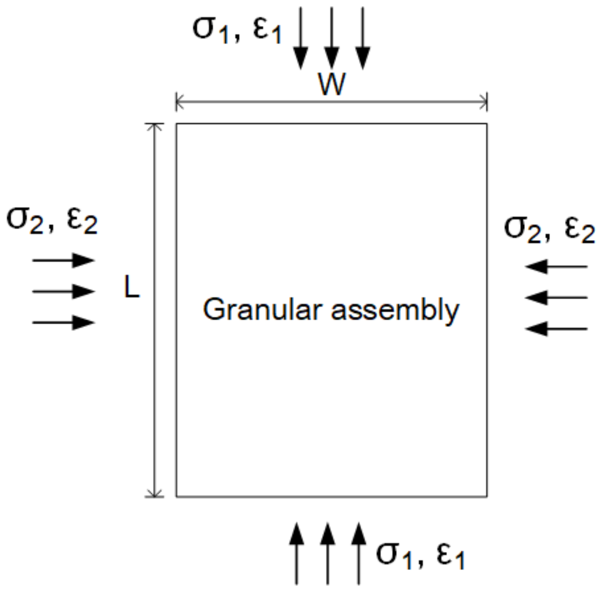

Figure 2: Schematic plot of DEM samples under the biaxial loading condition.

incremental strain definition used in this paper can be found in Liu et al. [52]. In Figure 3 and Figure 4, State D denotes the stress peak during biaxial loading, where several crossing shear bands firstly appear. Before State D, a strain structurization is already evident at small scale, and small crossing structures of relatively high incremental strain evenly distribute within the sample domain. These meso structures are observed in both experimental and numerical tests [41, 54, 47], and could be denoted as "incremental shear strain chain" from our previous work [49, 48]. After State D, two chronic shear bands finally form and the reflection is found at the left boundary, as shown in State E of Figure 4. Generally, the incremental deviatoric strain field is concerned to identify the strain localization of materials, and in Figure 4, the incremental volumetric strain field is also compared at the same stage. It can be seen that the incremental volumetric strain field demonstrates the same localized patterns as the incremental deviatoric strain field, and both the local dilation [4] (high negative value) and the local contraction (high positive value) concentrate within the local shear structures or shear bands. Therefore, not only shear deformation is triggered within the localization area, but also significant volumetric changes occur.

[4]in soil mechanics, the compression direction denotes the positive direction of strain, so the negative value of volumetric strain demonstrates dilation, and vice versa.

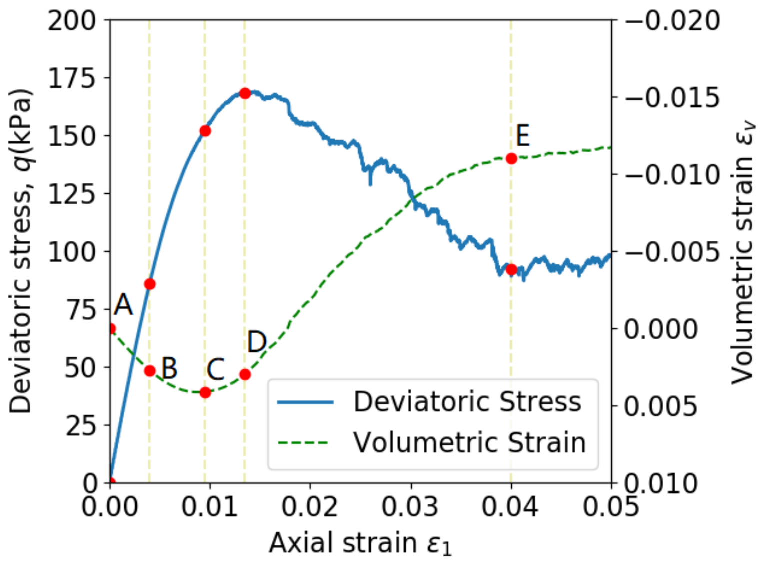

Figure 3: Deviatoric stress and volumetric strain evolutions of an example of the biaxial test (Sample DP in Appendix A). For the volumetric strain, the positive value denotes the compression and the negative value denotes the dilation of the sample.

3.2. Spatial distributions of contact sliding and particle rotation

In Section 3.1, the evolution of the incremental strain field of granular sample from homogeneous to heterogeneous patterns has been highlighted under biaxial loading. This evolution could be compared with the microscopic failures such as contact sliding and particle rotation.

The sliding behavior between two connected particles could be simply identified by Coulomb friction criterion in contacts in DEM simulations. When the tangential contact force $|f_t|$ reaches the limit of μf_n ($\mu = \tan\phi_g$ denotes the friction coefficient and f_n is the normal contact force), the two connecting particles will experience relative sliding at the tangential direction. Figure 5 presents the sliding contact distribution for the 5 key states shown in Section 3.1. Initially sliding contacts are scarce at State A; then the sliding distribution becomes denser and prone to give rise to the meso shear features (micro bands or shear chains); finally the sliding contacts concentrate evidently within the shear band. Visually, the clustered sliding behaviors are strongly correlated to the macro shear band at State E, however they show less significant features relative to meso shear structures before the stress peak, especially for States A and B. At State C and D, the sliding behaviors already exhibit some clustering features, and their distribution features should be further explored by adopting the shear chain concept.

Besides contact sliding, the incremental rotation of particles is proved to be related to the incremental strain field, especially for the period before stress peak and when the meso shear structures are fluctuating [43]. In this study, the positive rotation represents counterclockwise

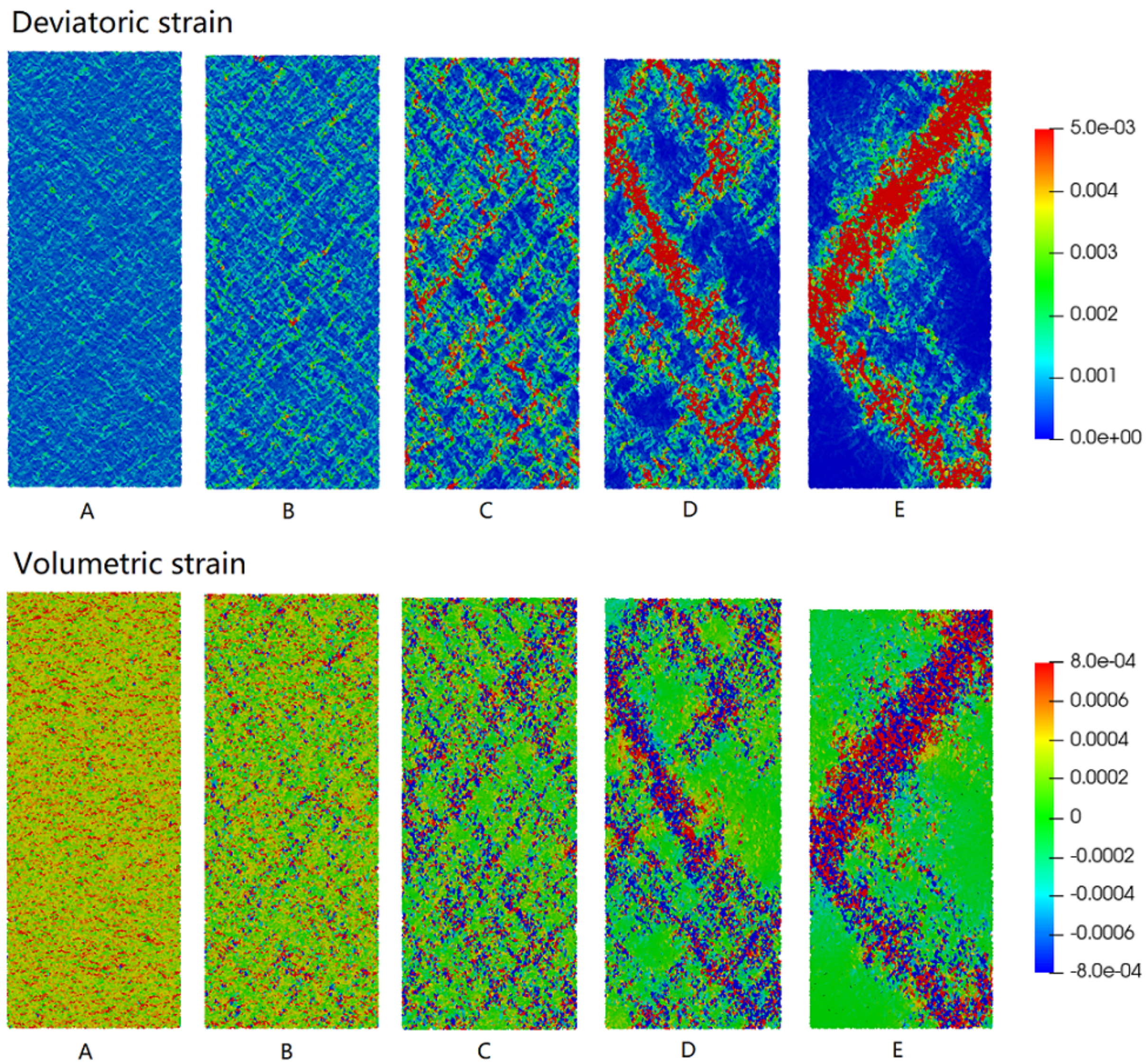

Figure 4: Spatial distributions of the incremental deviatoric and volumetric strain for different loading states in Figure 3. For the volumetric strain, the positive value denotes the compression and the negative value denotes the dilation.

direction and the negative rotation means the clockwise direction, and no background rotation is involved. Figure 6 shows the distributions of positive and negative particle rotation increments for the 5 states of Sample DP. Grey points shown in this figure denote particles with relative large absolute rotation increment (≥ 0.0005 rad, details of the threshold consideration are shown in Appendix B) between two steps (strain increment $d\varepsilon_1 = 0.0005$), which helps to distinguish the typical patterns of the distributions. Before the shear bands form (State A D), it can be seen that large positive and negative incremental rotation points are clustered with opposite preferred inclinations, which is also observed by other publications [43, 55, 56, 57]; however at State E, the patterns of both positive and negative rotation increments show accordance with

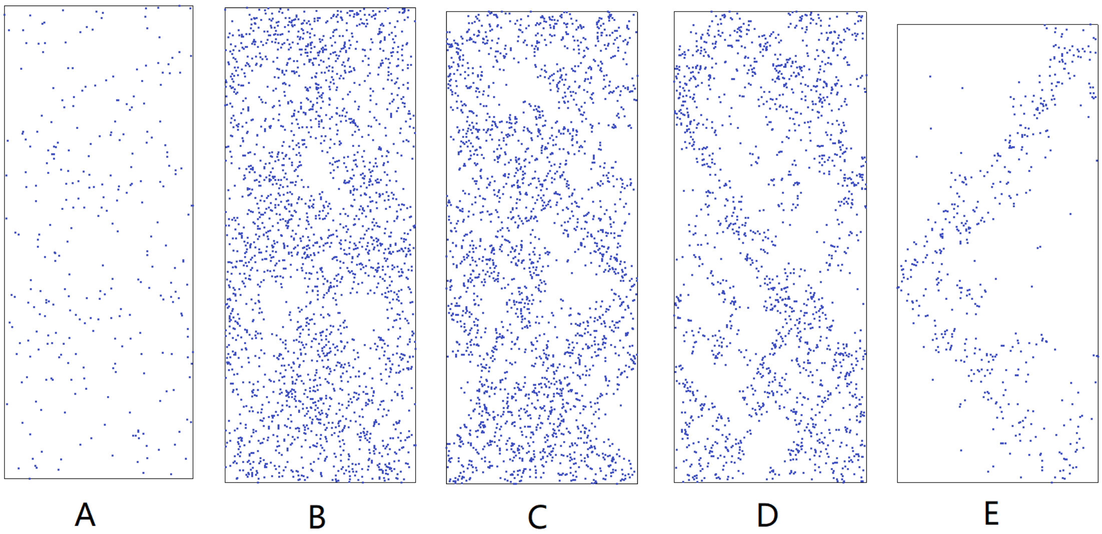

Figure 5: Spatial distributions of the contact sliding positions for different loading states.

the shear band area.

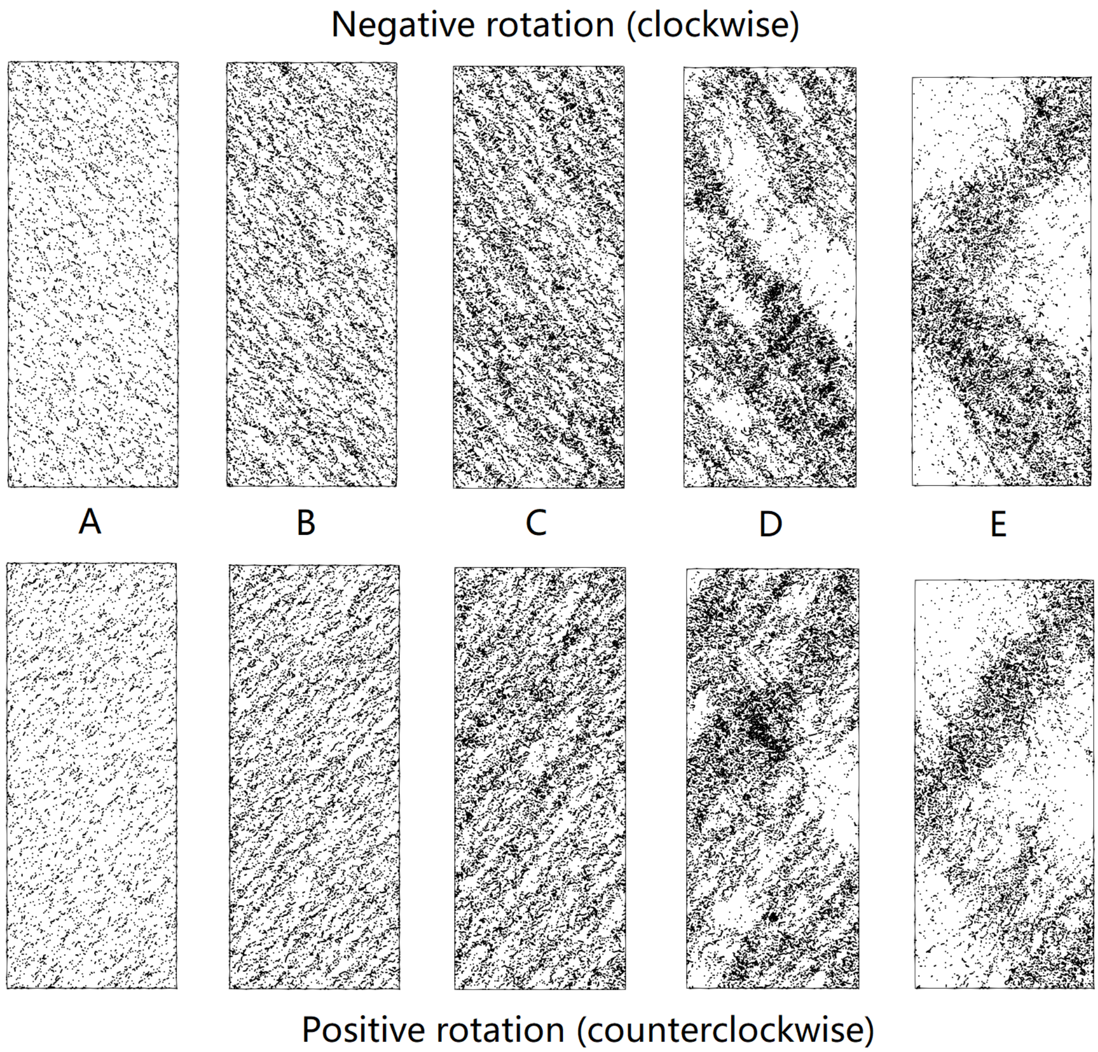

Figure 6: Spatial distributions of positive and negative particle rotation increments before stress peak for Sample DP in Appendix A.

To better exhibit the rotation distribution features, we define the mean incremental rotation of the particles belonging to a particular meso loop k [5]:

$$R_k = \frac{1}{A_k} \sum_{i=1}^{P_k} R_i A_i^{partial} \tag{2}$$

where A_k is the area of k, P_k means the particle number forming loop k, R_i is rotation increment of particle i, and $A_i^{partial}$ denotes the partial area of particle i included in loop k. R_k gives the information of the mean rotation increment at mesoscale and smooth the rotation increment fluctuating at the grain scale.

Figure 7 gives the distributions of the incremental rolling of loops for the 5 corresponding states. Similar but clearer than the pattern shown in Figure 6, the distribution of incremental rotation before State C not only corresponds to the strain field features shown in Section 3.1, but also exhibits the direction preference. In what follows, we name the shear structures "\\" as left slip structures, and the shear structures "//" as right slip structures. It is clear that left shear structures contain most clockwise particle rotation while right shear structures contain most counterclockwise particle rotation. As the biaxial loading processes, the local slip structures are no more diffusely distributed but more and more clustered until the final shear band emerges, which is clearly illustrated in Figure 7 from State C to State E. When the shear band finally forms, it can be observed that the average incremental rotation direction is consistent with the shear band orientation: at State E, two bands of right and left orientations contains mostly clockwise (red points) and counterclockwise (blue points) rotations respectively. Moreover, Figure 7 indicates that right shear bands also contain a noticeable fraction of counterclockwise rotation increment and vice versa. This highlights the fact that mesoscale rotations are not limited in one direction of a single band, which may be a sign that shear bands are composed of a collection of smaller mesostructures with different orientations (discussion in Section 6.2).

Based on those observations, we can preliminarily conclude that contact sliding and particle rotations are related to the meso shear structures and probably control the shear band initiation from the meso scale. As we have defined the "incremental shear strain chain" (briefly "shear chain") as the specific meso representative shear structures, in the following sections, we will

[5] Note that here the average rotation increment of one loop does not correspond to the rotation increment of the whole structure including void, R_k is considered for better showing the rotation features of meso slip structures with different directions.

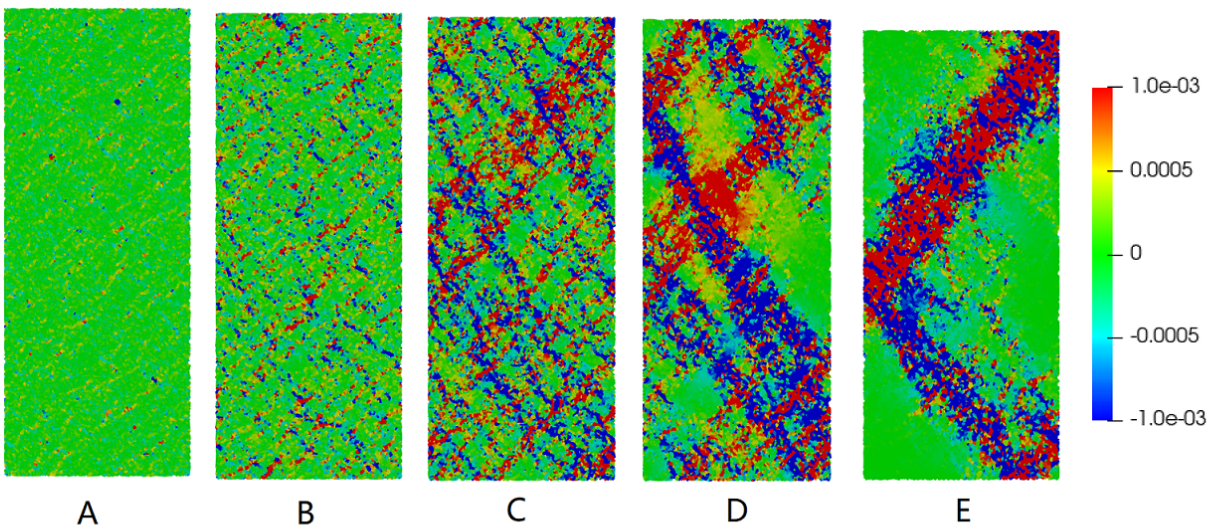

Figure 7: Spatial distributions of the large positive and negative incremental rotations of particles within Sample DP for different loading states (Positive: counterclockwise; Negative: clockwise).

use the shear chain concept to investigate the inmost mechanism.

4. Orientations of shear chains and shear bands

Inspired by force chain detection method [44, 45, 58, 50], the meso slips within granular materials have been defined as "incremental shear strain chains" in Liu et al. [49], which can basically describe the meso slip features within granular assemblies under shearing. Briefly, "incremental shear strain chain" is called "shear chain", denoting that meso loops with large incremental deviatoric strain are connected to form a single shear chain structure with the consideration of the shear and geometrical directions. The precise definition of shear chain is shown in Section 2, and more details can be found in Liu et al. [49].

Under deviatoric loading, the spatial diversity of shear chains are initially homogeneous and random in space before the development of shear bands. In Figure 8, a large number of shear chains at State B and C of the sample are presented with different colors. At States B and C, the stress peak is not reached yet and the kinematic pattern is still diffuse and fluctuating (Figure 4). Shear chains detected in Figure 8 denote the areas of large incremental deviatoric strain triggered by local shearing, which reflects the main features of the meso slip structure. The preferred orientation $< |\theta| >$ [6] of shear chains (proposed in Section 2) is near to $\pm 45°$ to the horizontal plane from the beginning of the loading, and State C seems to show a little larger

[6] When we talk about the orientation for shear chains or shear bands, the acute angle to the plane of major compression is considered.

value of this angle than that in State B since the shear band is becoming initiated. In fact, the orientation of shear chains corresponds to the stress ratio at the macro scale and is independent from the loading path, boundary conditions and void ratios of the granular material, which has been carefully investigated in our previous study [49, 48]. This is a material property ruled by the continuum mechanics principles.

Figure 8: Shear chain distributions within the sample for States B and C.

Unlike mesoscopic shear chains, shear bands denote a macroscopic band-like zone of finite thickness where large shear deviatoric strains are intensely distributed. In a continuum framework, this zone is delimited by strain discontinuity surfaces with continuous strain displacements.

Based on the classical theory, the inclination of shear bands is related to the internal friction angle φ and the dilatancy angle ψ of the material considered. The angle of shear band to the direction of minor principal stress is usually expressed as $\theta_{sb} = 45° + \frac{\varphi+\psi}{4}$. However, the boundary conditions may also have a strong influence on the shear band inclination, especially when the boundary is rigid. Then in a discrete framework with a piecewise constant strain field, characterizing the shear band domain is a challenging task which is too often achieved only by naked eyes.

In order to determine the orientation of the shear band in an objective way, the Standard Deviational Ellipse method can be used. This method has been widely applied in geography sciences [59], and defines an ellipse with a preferred orientation based on the local gathering data in space. Lehoucq et al. [60] used the similar method to detect the cracks of rocks. In this study, we firstly select loop cells with incremental deviatoric strains larger than a given threshold (in this paper it is set as the average value of deviatoric strain) with the group size n, i.e., the number of loop cells which are selected; then examine the distribution pattern of these selected cells by observation roughly. If the observed pattern of selected cells show the existence of a single shear band in a particular zone, we can identify the orientation of this shear band by the following method:

1. Get positions of n selected loop cells with large incremental deviatoric strain, and compute the following matrix:

$$\mathcal{M} = \begin{bmatrix} var(x) & cov(x,y) \\ cov(x,y) & var(y) \end{bmatrix} = \frac{1}{n} \begin{bmatrix} \sum_{i=1}^{n} \widetilde{x}_i^2 & \sum_{i=1}^{n} \widetilde{x}_i \widetilde{y}_i \\ \sum_{i=1}^{n} \widetilde{y}_i \widetilde{x}_i & \sum_{i=1}^{n} \widetilde{y}_i^2 \end{bmatrix} \tag{3}$$

   where x_i and y_i are the coordinates for each cell center, $\widetilde{x}_i = x_i - \bar{x}$ and $\widetilde{y}_i = y_i - \bar{y}$.

2. Compute the rotation angle of the ellipse γ

$$\tan\gamma = \frac{A+B}{C} \tag{4}$$

   where

$$A = (\sum_{i=1}^{n} \widetilde{x}_i^2 - \sum_{i=1}^{n} \widetilde{y}_i^2) \tag{5}$$

$$B = \sqrt{(\sum_{i=1}^{n} \widetilde{x}_i^2 - \sum_{i=1}^{n} \widetilde{y}_i^2)^2 + 4(\sum_{i=1}^{n} \widetilde{x}_i \widetilde{y}_i)^2} \tag{6}$$

$$C = 2\sum_{i=1}^{n} \widetilde{x}_i \widetilde{y}_i \tag{7}$$

3. The equation of the standard deviational ellipse is then

$$(\frac{x}{r_x})^2 + (\frac{y}{r_y})^2 = s \tag{8}$$

where

$$\begin{aligned} r_x &= \sqrt{2}\sqrt{\frac{\sum_{i=1}^{n}(\tilde{x}_i\cos\gamma - \tilde{y}_i\sin\gamma)^2}{n}} \\ r_y &= \sqrt{2}\sqrt{\frac{\sum_{i=1}^{n}(\tilde{x}_i\sin\gamma + \tilde{y}_i\cos\gamma)^2}{n}} \end{aligned} \tag{9}$$

and $s > 0$ denotes the size of the ellipse [7].

In the above equations γ relates to the shear band direction when n selected cells belong to the shear band domain. The absolute value of shear band angle θ_{sb} is considered here: when $\gamma > 0$, $\theta_{sb} = 90^\circ - \gamma$; when $\gamma < 0$, $\theta_{sb} = 90^\circ + \gamma$. An example of the application of the Standard Deviational Ellipse can be found in the left side of Figure 9. For samples with multiple shear bands, this method can be used for different segments of selected zones, which is shown in Figure 10.

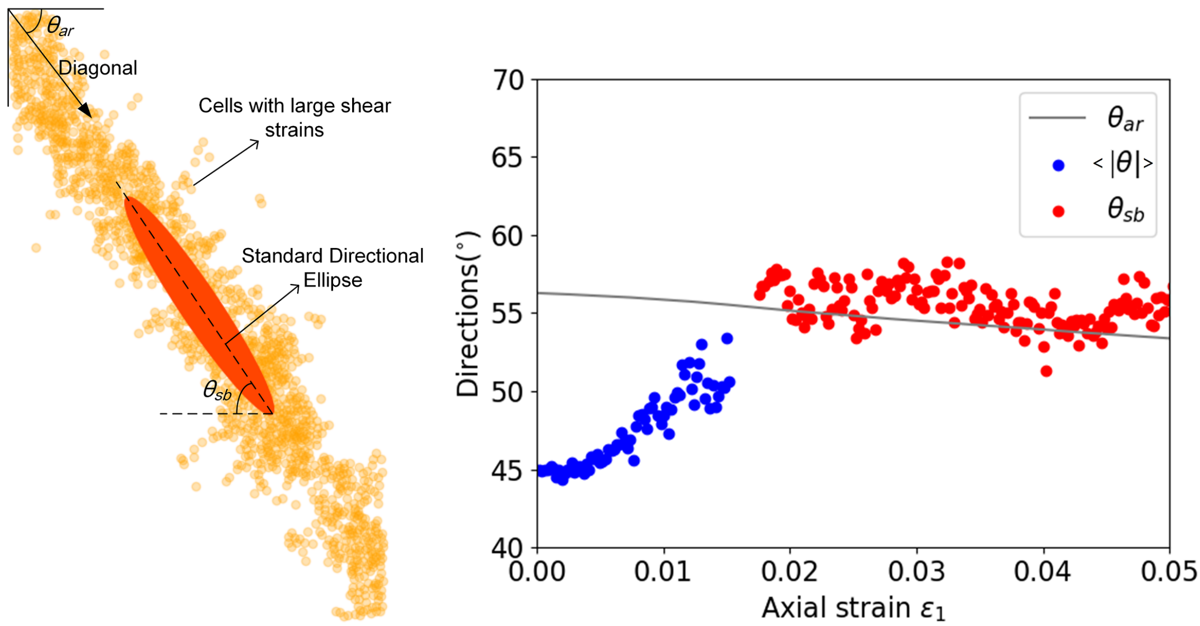

Figure 9: Example of single shear band (example of aspect ratio $L/W = 1.5$ in Appendix A) with the orientation determination based on the Standard Directional Ellipse method.

In Figure 9, the sample DF in Appendix A with a different aspect ratio $L/W = 1.5$ was selected to give an example of shear band orientation detection on the left side [8]. The evolutions

[7] s ($s > 0$) relates to the domain and density of data, and in this paper the value of s is not so important.

[8] It should be noted that the macro strain increment does not influence the evolution of shear chain and shear band orientations

of the average direction of shear chains $< |\theta| >$ (blue points) and the shear band θ_{sb} (red points) are compared along the shearing process in the right side. Since the final shear band seems to connect the diagonal corners of the sample, the diagonal angle θ_{ar} evolution is also shown in Figure 9. It can be seen that θ_{sb} and θ_{ar} is close for this condition. Before the shear band forms, the shear chain direction $< |\theta| >$ increases slightly from the beginning until the stress peak. After this stage, the shear chains are less easy to identify but the shear band orientation can be captured. The shear band orientation θ_{sb} is different from the initial mesoscopic shear chain direction $< |\theta| >$ dictated by continuum mechanics principles.

If we consider biaxial tests of different aspect ratios (see details in Appendix A), the shear band orientations seem not unique although the particle size distribution, the density and the loading path are almost the same. For example, the granular assembly of aspect ratio $L/W = 2.5$ (Sample DP) gives rise to two shear bands of different orientations, as shown in Figure 10. The upper shear band and the lower shear band show reflecting features on the left boundary, while the orientations of them exhibit some differences during whole loading process (Figure 10): on the left of the figure, the crossing position of the two bands is not at the midpoint of the boundary; on the right of the figure, θ_{sb-up} and $\theta_{sb-down}$ evolve with different angles to the horizontal plane. Comparing to Figure 9, Figure 10 and the shear band patterns of all the samples in Appendix A, it should be concluded that the shear band orientation is not unique for a sample with given initial density and particle size distribution. The shear band orientation is then influenced by the sample aspect ratio, as also observed for Sample DI, DK and DL in Appendix A (shear band orientation evolution curves are not shown here). It turns out from the above findings that the shear band orientation is not a material property as such, although intrinsic properties still have some impacts [61]. Even for a single shear band of a given sample, the shear band orientation is not uniform and locally some kinks may occur [62]. We can see that in Figure 9 and Figure 10, the boundary of shear bands is not smooth but involves small crossing structures, and during softening stage these crossing structures are evolving. Then the macroscopic shear band might be a mixture of shearing behaviors at a lower scale, and the proposed shear chains could be regarded as a proper material body with an intrinsic orientation independent of the sample aspect ratios [49].

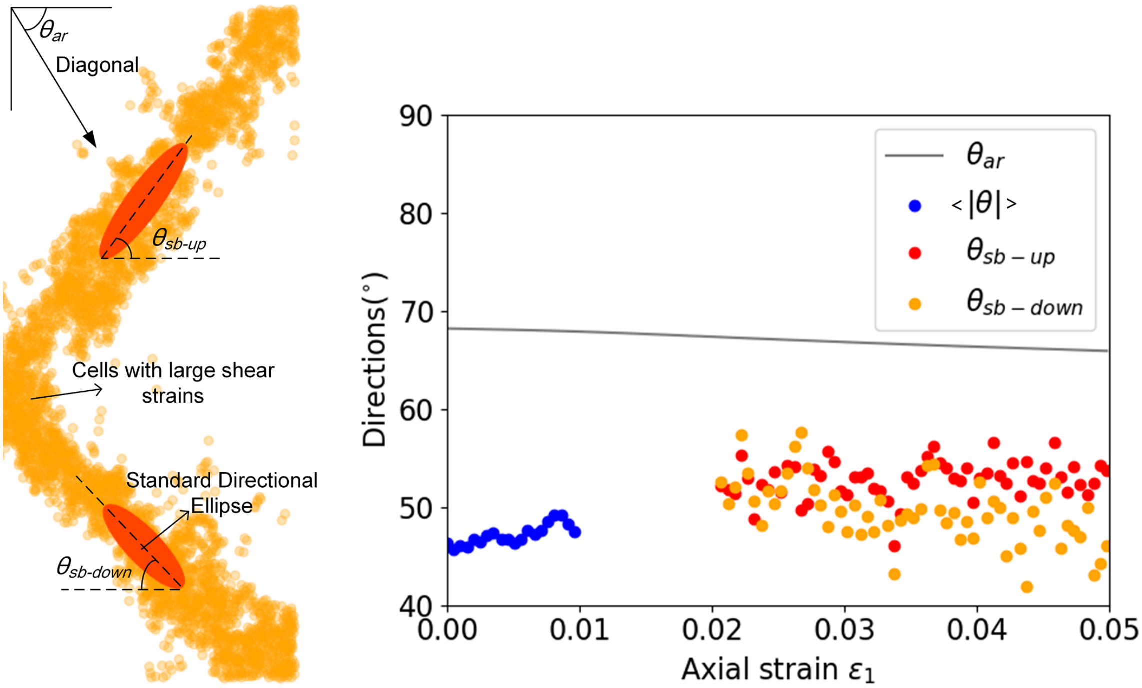

Figure 10: Granular sample with multiple shear bands of shear banding and evolutions of shear band and shear chain orientations($L/W = 2.5$).

5. Microscopic fabric, sliding and rotation in shear chain

5.1. Fabric anisotropy within shear chains

Within the granular assembly, particles are connected by contact with forces, forming a fabric network on the whole. The fabric tensor $\mathbf{\Phi}$, defined from the normal directions to the contact planes between particles, has been widely used to describe the contact orientation density distribution in granular materials [27, 63, 64]:

$$\Phi_{ij} = \frac{1}{N_c}\sum_{c=1}^{N_c} n_i n_j \tag{10}$$

where N_c is the total number of contacts within the granular system, and $\Phi_{ii} = 1$.

As shown in Figure 1, shear chains are defined based on loop tessellation where a part of contact network is involved. Then each contact loop is eligible to be described by its own fabric tensor, similarly to Eq. 10:

$$\Phi_{ij}^{l} = \frac{1}{N_c^l}\sum_{c=1}^{N_c} n_i n_j \tag{11}$$

where N_c^l is the total number of contacts within a given loop. Under 2D conditions, the fabric anisotropy of each loop a^l is related to the deviations between the major and minor principal values of the fabric tensor Φ_{ij}^l, i.e., $a^l = \Phi_1^l - \Phi_2^l$, where $\Phi_1^l = 0.5(\Phi_{11}^l + \Phi_{22}^l) + ((0.5(\Phi_{11}^l -$

$\Phi^l_{22}))^2 + (\Phi^l_{12})^2)^{0.5}$ and $\Phi^l_2 = 0.5(\Phi^l_{11} + \Phi^l_{22}) - ((0.5(\Phi^l_{11} - \Phi^l_{22}))^2 + (\Phi^l_{12})^2)^{0.5}$. In fact a^l describes the elongation of a given loop, the higher the value of a^l, the more elongated the shape of the loop [65].

In Figure 11, the evolutions of average fabric anisotropy for loops in shear chains A_{sc} and overall system A_{all} [9] are compared during biaxial loading (before shear banding). The 5 samples presented in Appendix A are selected for this analysis. It can be found that the average fabric anisotropy within shear chains shows mostly the unchanged trend along the deviatoric loading, while the average fabric anisotropy for the 5 samples overall stay increasing but lower than the shear chain anisotropy. The shear chain could be regarded as particular elongated zone with high average anisotropy in the granular assembly, irrespective to stress states and boundary conditions. In other words, the contacts in shear chain loops organized anisotropically in order to constitute meso shear structures.

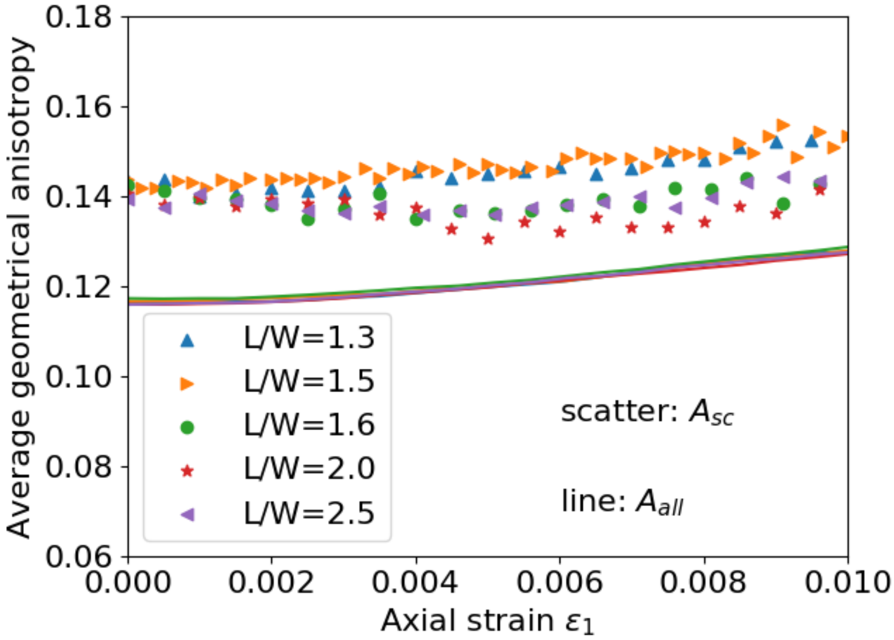

Figure 11: Average anisotropy comparisons for shear chain loops and overall system of 5 samples. Scatters are the anisotropy values for shear chains A_{sc}, and lines correspond to the anisotropy values of the overall system A_{all}. It should also be noted that nearly no difference can be found in A_{all} evolutions for the 5 samples.

5.2. Contact sliding statistics

At the macroscopic scale, failure occurs along a given loading path when a limit state is reached [46]. This means that for a particular choice of the loading parameters, a transition

[9] $A_{sc} = \sum a^l / N_{SCL}$ and $A_{all} = \sum a^l / N_{ALL}$, where N_{SCL} is the number of loops in all shear chains and N_{ALL} is the number of loops within the whole granular assembly

from a quasi-static to a dynamic regime can occur [66]. At the microscale, contact sliding corresponds to the microscopic failures between two grains with relative tangent displacement. Being able to correlate microscopic and macroscopic failures is the corner stone to explain the origin of strain localization. Liu et al. [40] pointed out that contact sliding can be correlated with force chain bending, and when strain localization occurs, sliding contacts only exist within the shear band.

Since the shear chain can represent the slip lines, it is tempting to check whether the correlation exists between the contact sliding and shear chain structures. Based on the shear chain definition, contacts can be grouped as follows:

- connection contacts (marked red in Figure 1) connecting two adjacent loops in shear chains, named "SCC"
- contacts in shear chains but not belonging to connection contacts (dashed lines connecting particles in Figure 1), named "SC"
- contacts not in shear chains, named "nonSC"

It should be noted that these 3 groups of contacts are mutually exclusive.

Evolutions of the average sliding index I_p ($I_p =< |f_t|/(\mu f_n) >$) for these 3 groups are shown in Figure 12, and 3 samples of different aspect ratios in Appendix A are considered. Connection contacts "SCC" hold the highest magnitude of sliding index I_p, followed by the shear chain contact group "SC" and non-shear chain contact group "nonSC" respectively. Therefore connection contacts are like *bridges* in shear chains, their higher probability of sliding indicating the important role of sliding contacts in mesoscopic shear structure forming. Although sliding contacts have a preferred direction close to the lateral confining direction [49, 67], their influence on the incremental strain field involves geometric rearrangements captured at the mesoscale by shear chains. This observation strengthens the interpretation of shear chains as slip lines in continuum materials [48].

5.3. Particle rotation within shear chains

In Section 3.2, the incremental particle rotation distribution has been compared with the incremental deviatoric strain field. It has been proved that clockwise rotation and counterclockwise rotation will concentrate along different (or opposite) orientations. Statistically, Figure 13

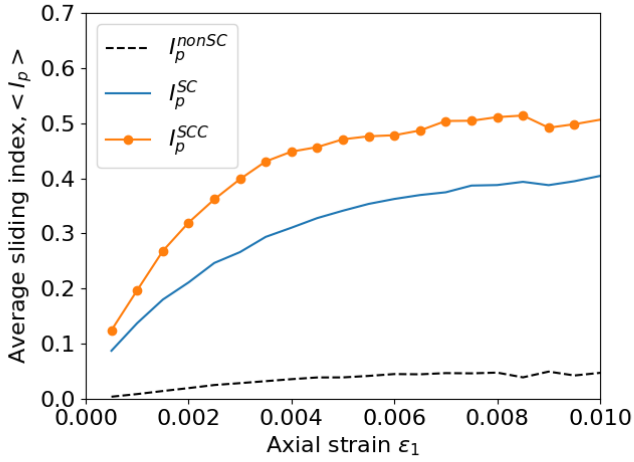

(a)

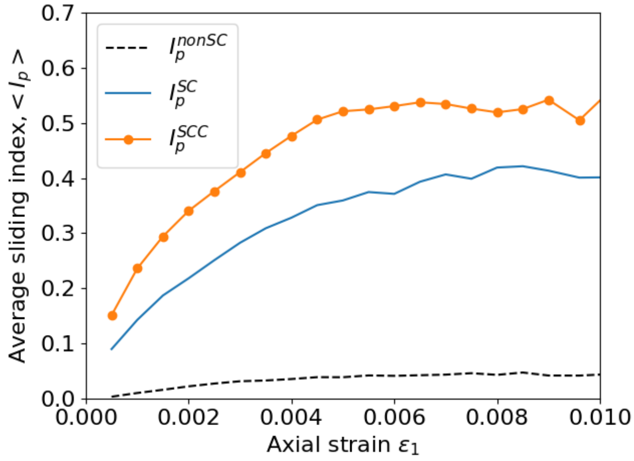

(b)

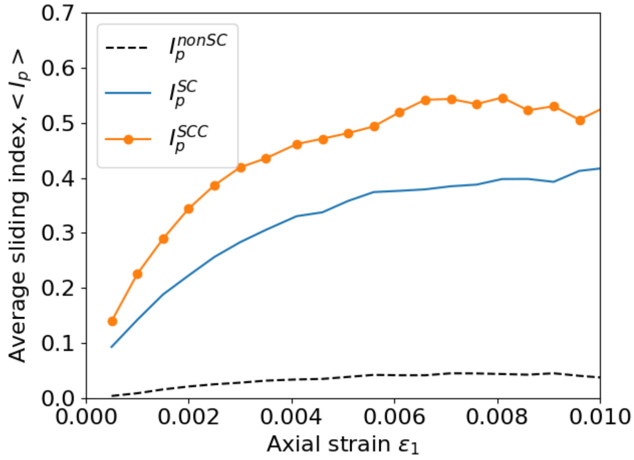

(c)

Figure 12: Average sliding index evolutions for connection contacts “SCC”, shear strain contacts “SC” and non shear chain contacts “nonSC”: (a) sample of aspect ratio $L/W = 1.3$;(b) sample of aspect ratio $L/W = 2.0$;(c) sample of aspect ratio $L/W = 2.5$.

10 shows the average rotation evolutions of particles within left shear chain (oriented like “\\”),

[10]The green fluctuation points are due to some free particles of large rotations within the whole sample

right shear chain (oriented like "//") and the overall system respectively for the sample of aspect ratio $L/W = 1.5$ (Sample DF in Appendix A). Particles in left shear chains almost own the negative value of rotation (clockwise) while particles in right shear chains have the mean rotation of positive value (counterclockwise), which corresponds to the observations in Section 3.2 and also reported in Wang et al. [43]. For the overall system, the average rotation is nearly zero due to the offset of positive and negative rotations in general. The defined shear chain is proved to be able to capture the rotation features of meso shear behaviors. This observation highlights the analogy between shear chains and slip lines where the slip motion generates rotation along the slip surface.

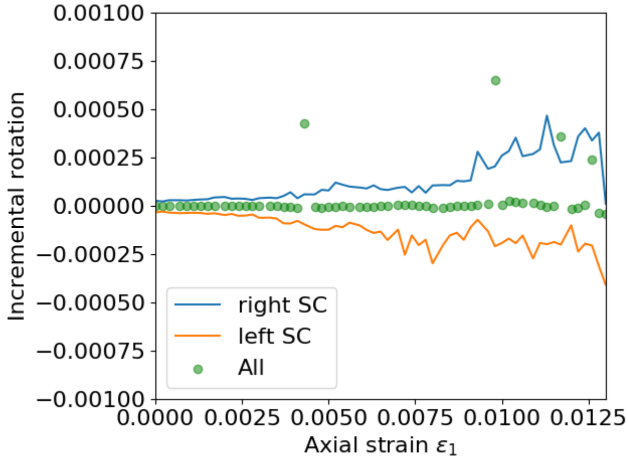

Figure 13: Average rotations for right shear chains "//", left shear chains "\\" and all shear chains. "SC" means "shear strain chain" for simplification.

Like different groups of contacts analysed in Section 5.2, particles can also be divided to different groups to investigate the particular rotation features. As shown Figure 1, all the particles involved in shear chains could be the "SC" particles; the particles colored in green which are in the connection positions in shear chains, they can be labeled as "SC connex" particles; while particles in shear chains but excluded by "SC connex" could be the "SC non-connex" particles which are not colored in the figure. For left shear chains and right shear chains, we plot the evolutions of average incremental rotation for "SC connex" contacts, "SC non-connex" contacts and "SC" contacts in Figure 14 for sample DF, respectively. Although the magnitudes of the 3 groups do not diverge significantly, the absolute values of incremental rotations are larger at shear chain connection positions. In other words, the grains undergoing different incremental rotation direction (clockwise and counterclockwise) could also play an important role in forming the meso shear structures, i.e., shear chains.

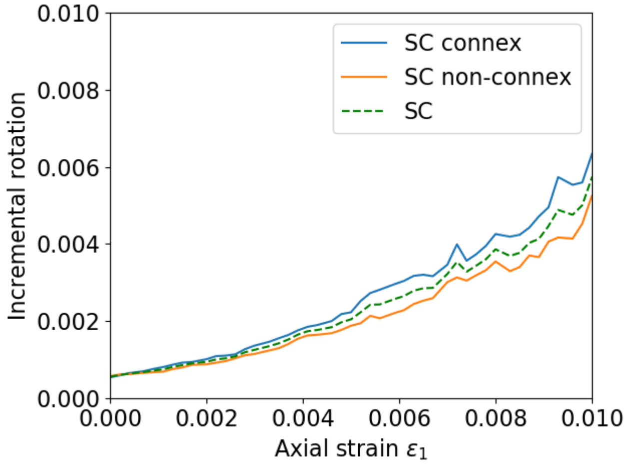

(a)

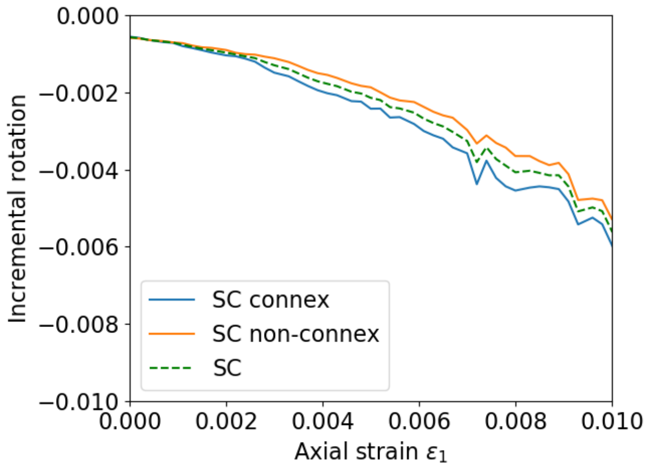

(b)

Figure 14: Average incremental rotation for particles in connection contacts (SC connex), not in connection contacts (SC non-connex) and in shear chains (SC): (a) right shear chains; (b) left shear chains.

In Figure 15, we select several shear chains near the initial state of biaxial loading, and particles of large absolute incremental rotation are highlighted together. The threshold 0.0005 rad (threshold details in Appendix B) is used to highlight large incremental rotations, and different colors denote the sense of rotation. Shear chains (a) and (e) are right shear chains, where positive incremental rotations (counterclockwise) frequently appear; on the contrary, shear chains (b)-(d) correspond to left shear chains where negative rotations (clockwise) mainly occupy the center in connection positions. Particles with large incremental rotations (both positive and negative) can be found for a particular shear chain, although the proportions and positions diverge. That explains why in Figure 14, the difference between the 3 groups is not very large. The shear chain (f) in Figure 15 is left chain with blue particles (clockwise rotation), moreover, several particles excluded by the shear chain (f) are also shown with counterclockwise rotation (orange color). The particles of orange color are connected along the opposite direction of shear chain (f) with quasi-linear feature, then the meso loops related to these particles could also form a shear chain but not detected in our current algorithm [49] since chain branches are not considered [11]. Since the crossing slip structures are obvious in the incremental deviatoric strain field (Figure 4), a given left shear chain is prone to be crossed by one or more right shear chains. Then the rotation near the crossing place might be mixed with both large positive and negative values, which causes the co-existence of counterclockwise and clockwise rotations for one shear chain.

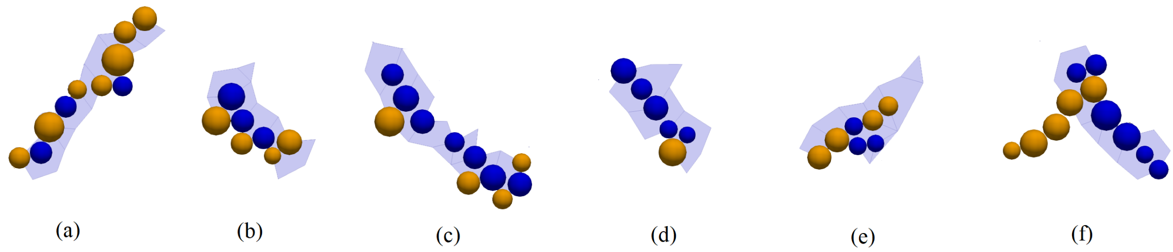

Figure 15: Examples of particles with large rotation (absolute value, orange denotes counterclockwise direction and blue denotes clockwise direction) and their spacial relations to the shear chains.

6. Discussion: links between multiscale shear behaviors

6.1. Shear chains and shear bands at different scales

Shear chains at meso scale can represent the meso slips during deviatoric loading. They relate to the concept of slip lines in plasticity (discontinuities in the displacement field), which is different from shear band (discontinuities in the strain field) [49, 48].

In Section 4, the orientation features are compared for shear chains and shear bands. Furthermore, the width and length are also important factors for comparison. In Figure 16, the zooming images of the shear strain field for shear chain area and shear band area are given for Sample DF. It can be observed that thin and quasi-linear shear chains are composed of loops with large incremental deviatoric strain, resulting in the width around a few times the particle diameter. While for the width of shear bands, it should be dozens of particle diameters

[11] In Liu et al. [49], we developed the method for searching shear chains. Similar to the definition of force chains [44], the current algorithm for capturing shear chains is not perfect because only one branch can be extracted when the crossing point is met. Despite all this, significant features of shear chains are already well described by using the current method [49]. In our future work, the shear chain detection method will be improved from a topological perspective.

according to some publications [40, 68]. Besides, the direction of the incremental displacement of the particles is shown with unit arrows in Figure 16. It can be noted that the direction of the displacement field is slightly tilted when crossing the shear chain. As for the shear band, the incremental deviatoric strain field exhibits large fluctuations, and vortices exist as highlighted by the incremental displacement directions in Figure 16(b). These observations are consistent with results reported in [19, 69], indicating that shear chain and shear band are involved with different micro-structural features.

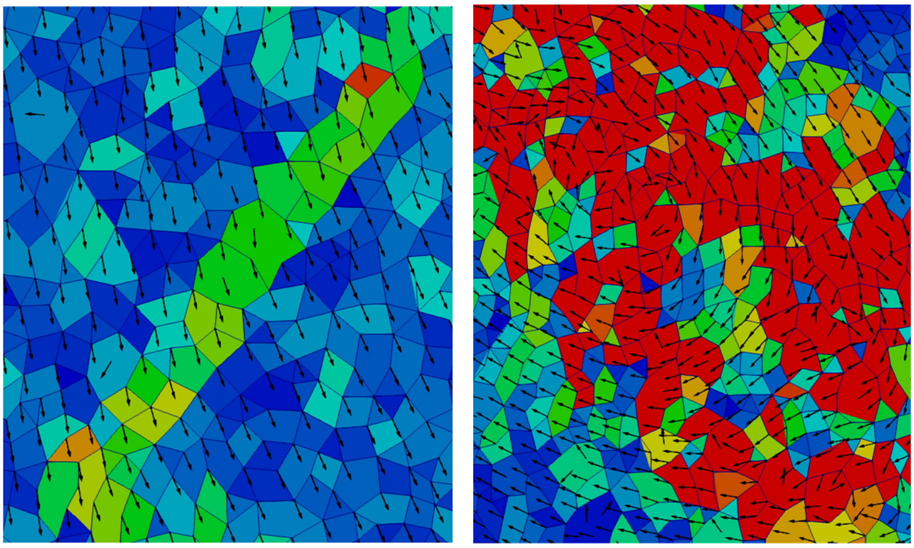

(a) (b)

Figure 16: Zoomed images of incremental strain fields compared to the direction of the displacement field: (a) domain of a meso shear structure; (b) part domain of shear band.

According to the investigations till now, Table 1 reports the differences between these two structures. The length and width of shear chains and shear bands are described by the average diameter D_{50} of the granular samples. The shear chain length is evolving during the biaxial shearing, with a slight increasing trend.

Content	Shear band	Shear strain chain
Width	8-40 D_{50}	1-3 D_{50}
Length	Size of specimen	Several D_{50},evolving
Direction	Affected by slip direction and boundary	Unique, maybe related to plastic theory
Displacement field	Evident vortex	Small rotation

Table 1: Comparisons of the shear band and the shear strain chain.

Although shear band and shear strain chain are different in terms of scales, they can be correlated under some reasonable assumptions. Shi and Horii [70] firstly proposed a simple microslip model to describe the origin of shear banding in sand deformations by assuming internal defects within the specimen. In recent years, meso Mohr-Coulomb theory has been adopted in describing the mesoscopic shear behaviors of amorphous materials [54, 71]. Houdoux et al. [47] used two incremental scales (fast and slow temporal correlations) to explain the evolutions of shear banding and micro-bands. Darve et al. [48] demonstrated that meso slip lines and shear bands are distinct localized objects and discussed why and how the network of meso-slip lines is bifurcating into a set of few macro-shear bands. The literature agrees that the mesoscopic shear structure (micro-band or shear chain) and the ultimate chronic shear band exhibit different geometrical and mechanical features, and it is often proposed that the meso shear structures may aggregate in a dense distribution within the shear band to create this larger structure. Therefore, we believe that shear band and shear chain should be strongly correlated. Combining the micro failure distribution features analysed in Section 5, we can assume the shear chain concept as the bridge connecting shear behaviors of multiscales.

6.2. Bridging role of shear chains

In Section 3, the microscopic failures are shown to concentrate within the shear band; and in Section 5, the microscopic failures are proved to be correlated to the meso shear chain formation. Therefore we can conjecture that meso shear chains triggered by sliding and rotation are concentrated within shear bands. According to the present analysis and some literature review (such as Houdoux et al. [47]), the possible relations between shear chains and shear bands are drawn in Figure 17. Figure 17(a) corresponds to a regular arrangement of shear chains and Figure 17(b) corresponds to a collection of shear chains of symmetric orientations (with respect to the axial direction) in shear bands.

Figure 18 shows an example of the spatial distribution of large counterclockwise and clockwise incremental rotations for a shear band within a granular sample (Sample DF in Appendix A). Within the shear band, particles with large rotation increments of different directions are not arranged in order by two preferred orientations in Figure 18. At the stages before shear banding, the incremental rotation fields are corresponding to shear chains of opposite orientations, as shown in Figure 6 and Figure 7; examples in Figure 15 further demonstrate the correlation between shear chains and particle rotations. Therefore, a stochastic-structured pattern of shear chains in shear bands could be proposed from the perspective of kinematic rotation features, which demonstrates that Figure 17(b) could approach the real situation. This hypothesis is also supported by the fact that inside the shear band, the normal displacement field shows large

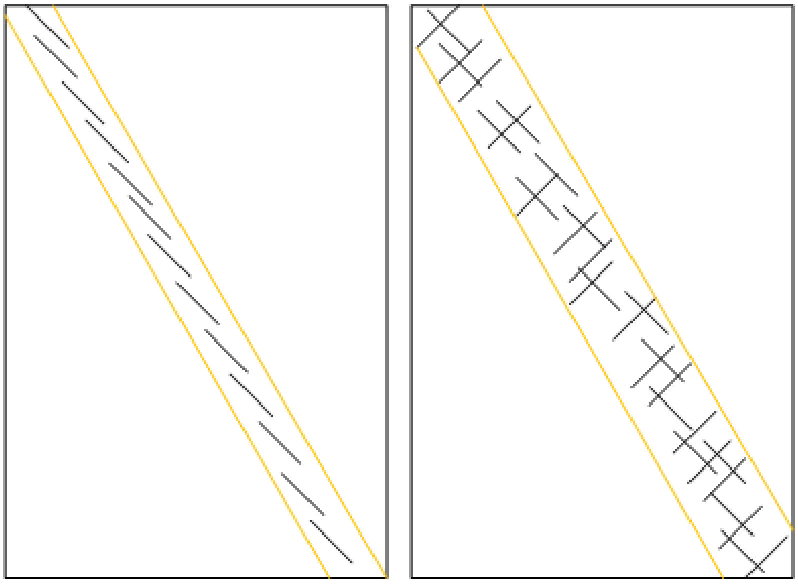

(a) (b)

Figure 17: Schematic representation of the relationship between shear band and shear chains. Shear chains are denoted by dark straight short lines and the shear band zone is between the two yellow lines. Case (b) is conjectured to approach the actual situation compared to Case (a).

variations even vortices. As shown in Figure 16(b) and reported in literature [69], shear chains (or microbands) oriented in only one preferred direction could not induce large fluctuations like vortices. Houdoux et al. [47] also reported the same observation according to the spatial and temporal correlation analysis.

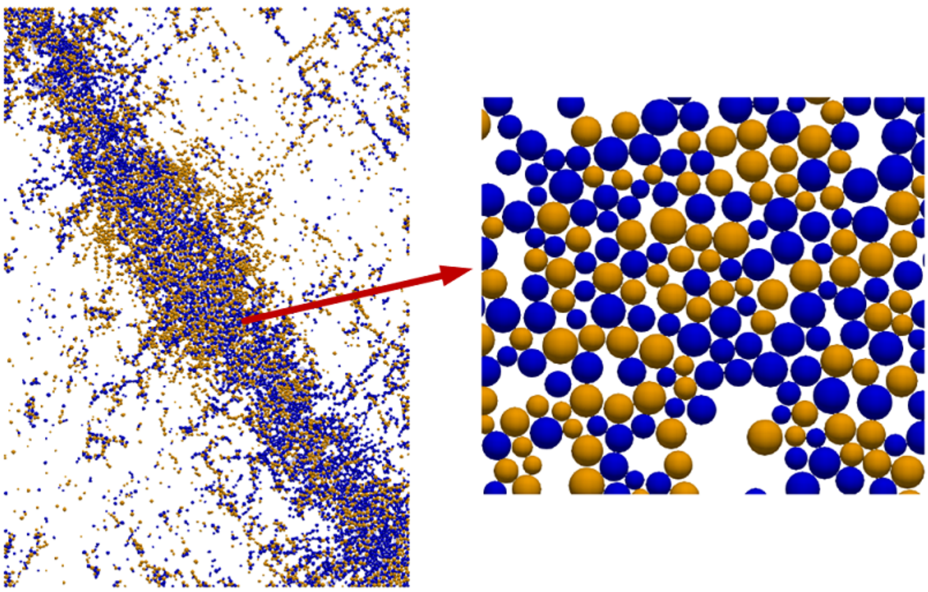

Figure 18: Particles of large incremental rotations (the orange denotes counterclockwise direction and the blue denotes clockwise direction) for a state when the shear band forms.

As shear banding has been a concerned issue in geomechanics for a long time, microscopic or mesoscopic representations inside the shear band have been studied from various perspectives.

For example, it has been shown that force chains rotate and bend inside shear band [52], sliding contacts and rotations accumulate inside the shear band [40, 62], and meso loops of large size appear inside shear band [11]. We define the shear chains as meso slips to represent the strain localization phenomena before shear band occurs [49], and manage to correlate this meso shear structure to shear behaviors at macro and micro levels. According to the analysis in this paper, the difference between shear band and shear chain has been clarified and the roles of microscopic shear behaviors on shear chains are preliminarily identified. Since microscopic failures commonly occur inside the shear band and they may trigger the shear chain formation, we assume that shear chains should be randomly distributed within the shear band, as illustrated in Figure 19. Microscopic failures such as sliding and particle rotation play key roles in forming shear chain structure (on the right of Figure 19), since the connection positions are commonly controlled by sliding contacts and particles of large rotation. The bridge from micro to macro shear behaviors could therefore be related to the meso shear chains. Shear chains could provide a missing link between micro to macro shear behaviors.

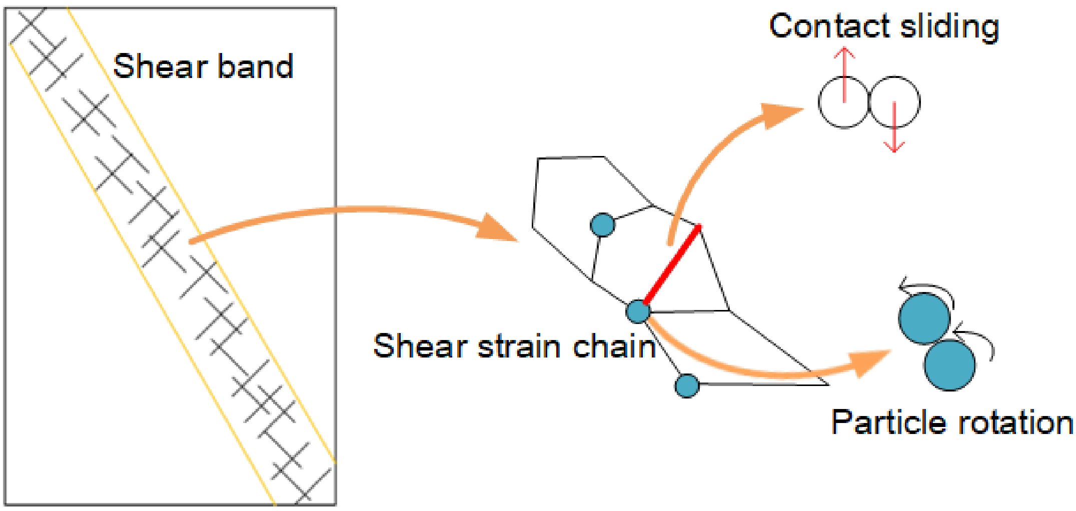

Figure 19: The bridge role of meso shear strain chains from microscopic to macroscopic shear failures.

This is our preliminary study and assumption of the bridge role of shear chains in linking macro and micro behaviors, and future work is necessary in terms of theory development and verification in 3D real cases, for example. Besides, we only considers the pure rotation of particles in this paper, the adaption of shear chains on the system with background rotation, as discussed in Singh et al. [72], should be further investigated.

7. Conclusion and outlook

This paper deals with the shear behaviors at micro, meso and macro scales in granular materials and relates them thanks to the concept of shear strain chain defined in our previous studies [49, 48]. A series of DEM biaxial tests are considered, providing rich detailed information on the multiscale shear features. Shear chains are proved to be influenced by the concentration of contact sliding and particle rotation, and they generally keep a steady anisotropy. Shear bands are failure zones of a higher scale, and are shown to be very sensitive to sample aspect ratios. Results presented in this paper support the idea that shear bands forms as a collection of shear chains in a given domain driven by boundary effects. Meticulously, we conclude as follows:

1. During the biaxial loading process of densely packed granular materials, both the incremental deviatoric and volumetric strain fields experience the transition from meso-scale diffuse localization to the final shear band. The spatial distributions of microscopic contact sliding and particle rotation also confirm this trend.

2. The method based on the Standard Deviation Ellipse is used to measure the shear band orientation. The orientations of shear chains and shear band are different, as shear chains are mesoscopic features governed only by material properties while shear band orientation are even more influenced by the aspect ratios of the rigid boundary.

3. In shear chains, average contact fabric anisotropy is kept almost steady and higher than the anisotropy of the overall system. Contact sliding mostly occurs in the connection contacts of shear chains. Particles of large rotation increment are frequent inside shear chains, and these particles of opposite rotating directions are associated with shear chains of opposite orientations, behaving as the main kinematic mechanism within shear chains.

4. Shear chains are different from the macro shear band in terms of thickness, orientation, theoretical background and relations to displacement field. As contact sliding and particle rotation are at the connection positions in shear chains and they also have a strong spatial correlation to the shear bands, we conjecture that shear chains may be included inside the developing shear band with the disordered distribution and shear chains appear therefore as a bridge between micro and macro shear behaviors.

This paper presents the preliminary study on the bridging role of shear chains, which have been defined as the shear structures at the meso scale [49]. Although qualitative findings are obtained for 2D granular systems under biaxial loading, we still need to extend our conclusions to more general conditions, for example, the 3D case and the complex loading path. The existence of shear chains for critical conditions, e.g., the minimal sample size and the minimal strain increment, should be clarified. The projection method [73] can be considered in the future work, to better discern the shear band orientation differences. In addition, we need to develop the theory for shear chains in granular materials, and reveal the mysterious origin of shear banding by combining other characterizations such as the vortex and force chain analysis. There are some cases where shear bands are prevented but shear chains emerges, e.g., periodic boundary and loose sample, how the meso shear chains will transfer during this failure process should also be the interesting future work.

Acknowledgements

This work was supported by Zhejiang Provincial Natural Science Foundation of China under Grant No. LY22E090002 and National Natural Science Foundation of China under Grant No.51909194 and No.51808193. The authors express their sincere thanks to the International Research Network GeoMech (IRN CNRS) for promoting positive and convivial interations among the authors of the present paper. The helpful suggestions from editors and reviewers on the quality improvement of our paper are really appreciated.

Appendix A. Biaxial tests of different boundary conditions

For this study, a set of quasi-2D [12] biaxial drained tests of samples with different aspect ratios (length vs. width) are conducted. Firstly, all specimens were randomly generated within large rectangular domains of prescribed aspect ratios, before being compacted by moving the bounding boundaries to a prescribed isotropic confinement. As shown in Figure 2, the aspect ratio is represented as L/W, where L denotes the length and W denotes the width. Rigid walls were set as boundaries. Although the specimen sizes are different, the particle size distribution is kept almost the same. The unique uniform distribution is chosen for each specimen, and the ratio of the maximum diameter to the minimum D_{max}/D_{min} is nearly 1.98 with the average

[12] by considering a single layer of 3D particles

size $D_{50} = 8.4$ mm. For other parameters in the DEM simulations, the material density is set to $\rho = 3,000$ kg.m^{-3}, k_n/D_s is set to 300 MPa, where $D_s = 2R_1R_2/(R_1 + R_2)$ and R_1, R_2 are the radii of particles in a given contact, and k_t/k_n is set to 0.5. All the specimens are compacted to a desired isotropic stress state with confining pressure of $\sigma_0 = 100$ kPa. During compression process, the contact friction angle between particles for each sample is set as 2° to reach a relative dense state. Gravity is not considered, and the boundary conditions are set as rigid frictionless walls. After this isotropic compression, the friction angle ϕ is set to 35° for the biaxial deviatoric loading. During the biaxial loading, the inertial number $I = D_{50}\dot{\gamma}\sqrt{\rho/p_0}$ [13] is lower than 2×10^{-6} which is small enough to meet quasi-static requirement.

The sample parameters for the drained biaxial tests are summarized in Table A.1. For those 16 samples, only the aspect ratio L/W and the particle number are different at the initial compacted states. The slight changes in void ratio V_r can be neglected. The sample chosen in Section 2 is Sample DP. When conducting the drained biaxial loading, a compression is imposed in the vertical direction with a constant strain rate of $\dot{\varepsilon}_1 = 0.01$ s^{-1} and the lateral pressure is maintained constant to $\sigma_2 = 100$ kPa.

Sample	L/W	N_p	D_{max}/D_{min}	D_{50}	Initial void ratio V_r
DA	1.0	13333	1.98	8.4 mm	0.0162
DB	1.1	14667	1.98	8.4 mm	0.0161
DC	1.2	16000	1.98	8.4 mm	0.0161
DD	1.3	17333	1.98	8.4 mm	0.0161
DE	1.4	18667	1.98	8.4 mm	0.0161
DF	1.5	20000	1.98	8.4 mm	0.0161
DG	1.6	21333	1.98	8.4 mm	0.0161
DH	1.7	22667	1.98	8.4 mm	0.0160
DI	1.8	24000	1.98	8.4 mm	0.0161
DJ	1.9	25333	1.98	8.4 mm	0.0160
DK	2.0	26667	1.98	8.4 mm	0.0160
DL	2.1	28000	1.98	8.4 mm	0.0160
DM	2.2	29333	1.98	8.4 mm	0.0160
DN	2.3	30667	1.98	8.4 mm	0.0160
DO	2.4	32000	1.98	8.4 mm	0.0159
DP	2.5	33333	1.98	8.4 mm	0.0159

Table A.1: Sample parameters of drained DEM tests.

Under biaxial loading, the overall stress-strain responses of the drained biaxial tests of different L/W are shown in Figure A.1. It can be observed that nearly no differenct can be found for the deviatoric stress evolution curves before the stress peak state (the onset of

[13] D_{50} denotes the average diameter;$\dot{\gamma}$ is the shearing rate; p_0 means the average stress.

softening) of 16 samples, and the large divergences after the stress peak could be attributed to the bifurcation development.

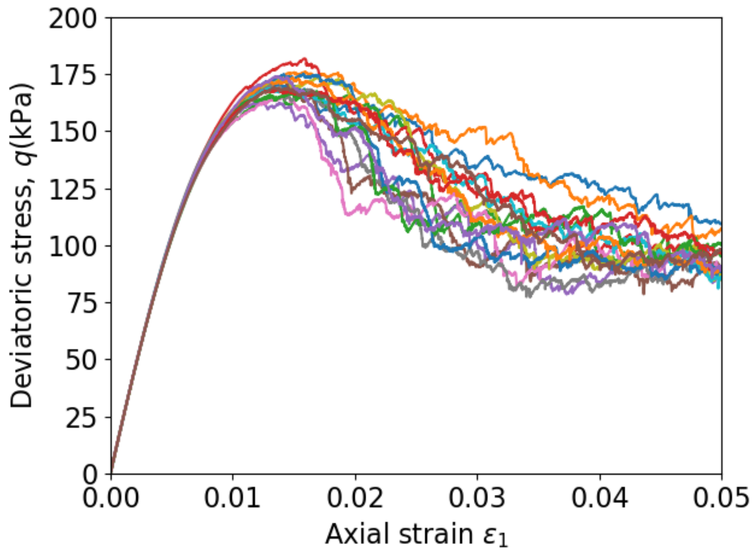

(a)

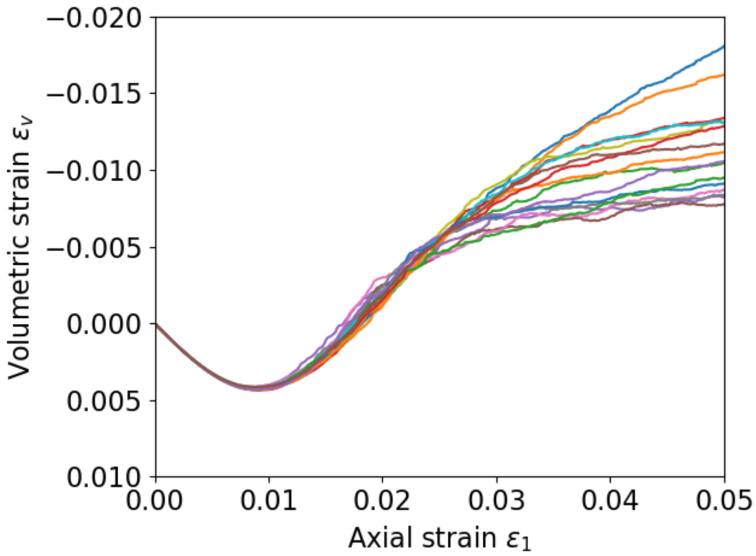

(b)

Figure A.1: Evolutions of deviatoric stress q (a) and volumetric strain ε_v (b) during drained biaxial tests with axial strain rate $\dot{\varepsilon}_1 = 0.01$ s^{-1} and lateral confinement $\sigma_2 = 100$ kPa. Different curves correspond to different aspect ratios L/W. We ignore the labels of the samples since all the curves share the same period before the stress peak.

For all the drained biaxial tests of dense samples, chronic shear band appears from the point near stress peak to the final state. The patterns of shear bands are diverse, as shown in Figure A.2. Under some conditions, a single shear band is identified (aspect ratio L/W=1.4, 1.5, 1.6, 1.7, 2.0 and 2.1); while multiple shear bands with reflections can be found for other cases. It is clear that the shear band event does not hold unique features when the aspect ratio is changed.

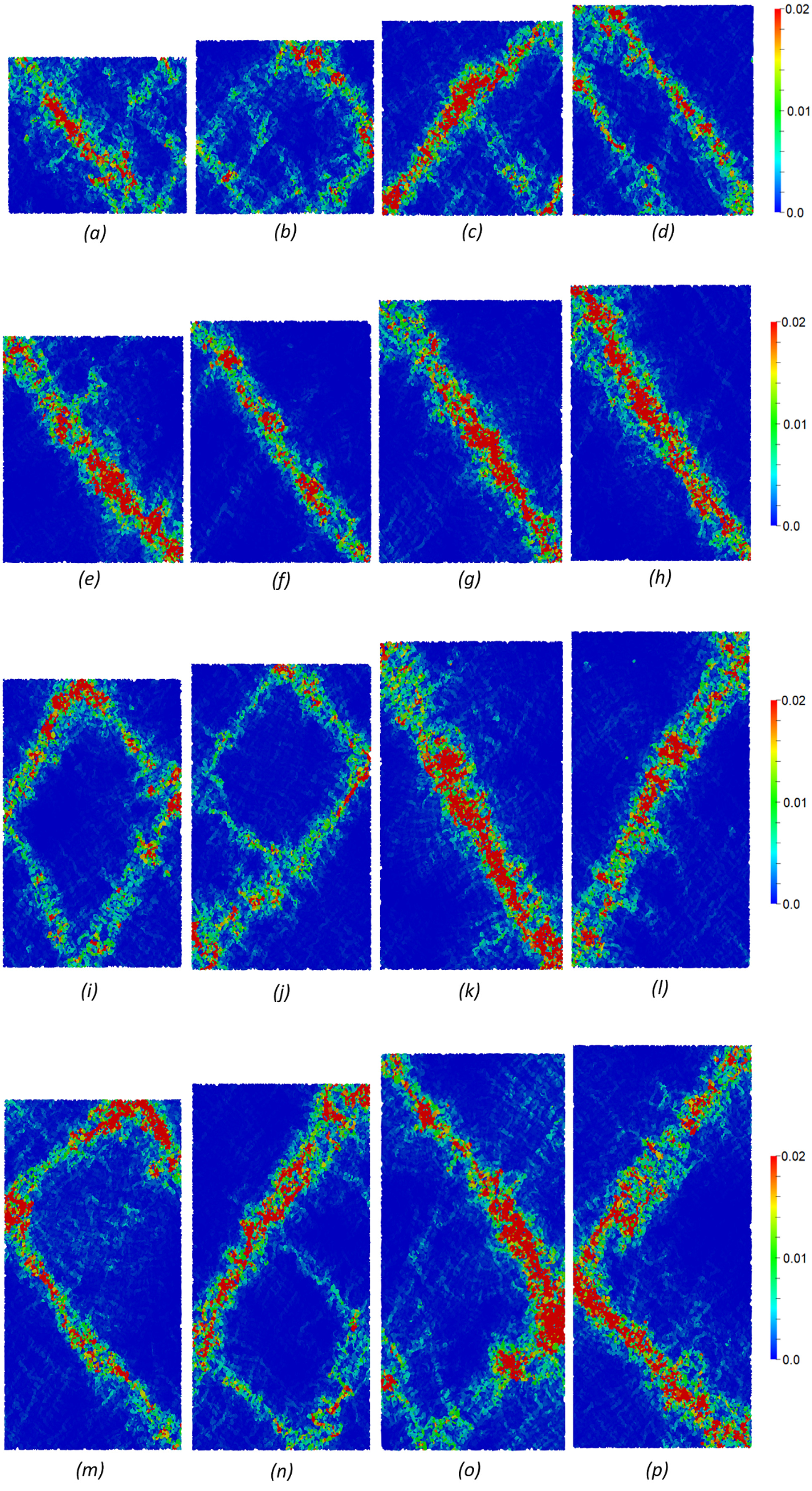

Figure A.2: Shear band patterns for specimens of different aspect ratios: (a)$L/W = 1.0$; (b)$L/W = 1.1$; (c)$L/W = 1.2$; (d)$L/W = 1.3$; (e)$L/W = 1.4$; (f)$L/W = 1.5$; (g)$L/W = 1.6$; (h)$L/W = 1.7$; (i)$L/W = 1.8$; (j)$L/W = 1.9$; (k)$L/W = 2.0$; (l)$L/W = 2.1$; (m)$L/W = 2.2$; (n)$L/W = 2.3$; (o)$L/W = 2.4$; (p)$L/W = 2.5$.

Appendix B. Threshold of large rotation increments in sheared granular assembly

In this paper, a number of quantities for meso or micro structures are calculated by the incremental form. All the increments are compared by two successive states with the macro strain increment of 0.0005, as well as the incremental rotation of particles. When defining particles of large rotation increment (absolute value) in this paper, a threshold 0.0005 rad is used. The chosen value results in clear images of featured patterns of rotation increment field. Figure B.1 gives an example of rotation increment distributions by using different thresholds for Sample DP in Appendix A at State B. When the threshold is too small (0.0001 rad) or too large (0.01 rad), the featured pattern of rotation increment field can not be well captured. We choose the value of 0.0005 rad to measure the large rotation increment in this paper, since the field pattern is clear and a large number of particles are included. It should be noted that the threshold 0.0005 rad is applicable for simulations of this study, when considering other cases a new threshold should be given with the respect to the strain increment between two successive states.

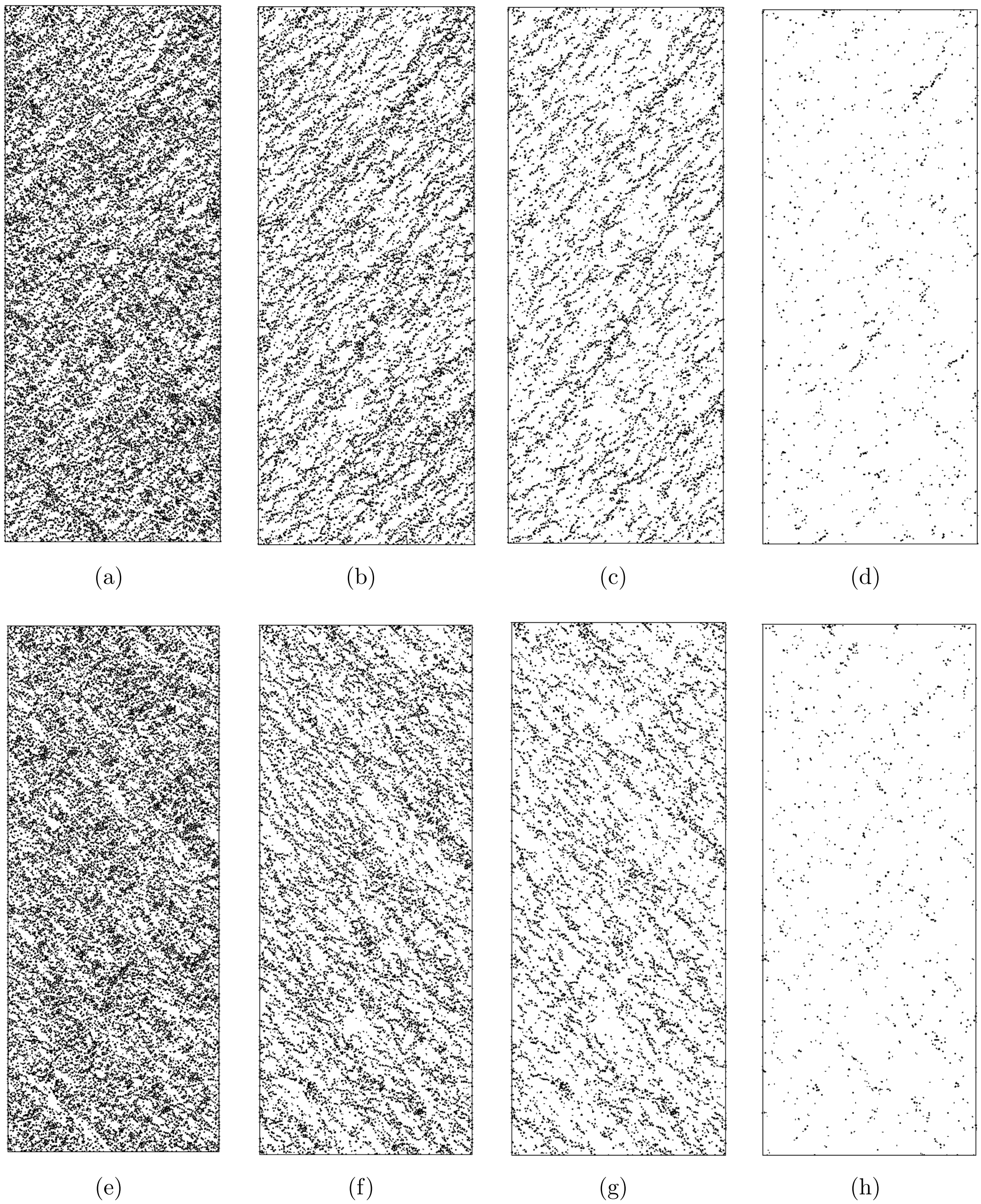

Figure B.1: Distribution maps of particles with large rotation increments. Different thresholds are set as: threshold 0.0001 rad for (a) positive and (e) negative rotation increment; threshold 0.0005 rad for (b) positive and (f) negative rotation increment; threshold 0.001 rad for (c) positive and (g) negative rotation increment; threshold 0.005 rad for (d) positive and (h) negative rotation increment.

References

[1] S. Taylor, E. Brodsky, Reversible compaction in sheared granular flows and its significance for nonlocal rheology, Geophysical Research Letters 47 (2020) e2020GL087137.

[2] Y. Jiang, G. Wang, T. Kamai, M. J. McSaveney, Effect of particle size and shear speed

on frictional instability in sheared granular materials during large shear displacement, Engineering Geology 210 (2016) 93–102.

[3] A. Schofield, P. Wroth, Critical state soil mechanics, McGraw-hill, 1968.

[4] Z. Yang, Y. Wu, Critical state for anisotropic granular materials: a discrete element perspective, International Journal of Geomechanics 17 (2017) 04016054.

[5] W. Zhou, J. Liu, G. Ma, X. Chang, Three-dimensional dem investigation of critical state and dilatancy behaviors of granular materials, Acta Geotechnica 12 (2017) 527–540.

[6] X. S. Li, Y. F. Dafalias, Dilatancy for cohesionless soils, Geotechnique 50 (2000) 449–460.

[7] R. Wan, P. Guo, A simple constitutive model for granular soils: modified stress-dilatancy approach, Computers and Geotechnics 22 (1998) 109–133.

[8] Y. Xiao, M. Meng, Q. Chen, B. Nan, Friction and dilatancy angles of granular soils incorporating effects of shearing modes, International Journal of Geomechanics 18 (2018) 06018027.

[9] P. V. Lade, Instability, shear banding, and failure in granular materials, International Journal of Solids and Structures 39 (2002) 3337–3357.

[10] F. Nicot, F. Darve, Diffuse and localized failure modes: two competing mechanisms, International Journal for Numerical and Analytical Methods in Geomechanics 35 (2011) 586–601.

[11] H. Zhu, H. N. Nguyen, F. Nicot, F. Darve, On a common critical state in localized and diffuse failure modes, Journal of the Mechanics and Physics of Solids 95 (2016) 112–131.

[12] F. Radjai, J.-N. Roux, A. Daouadji, Modeling granular materials: century-long research across scales, Journal of Engineering Mechanics 143 (2017) 04017002.

[13] J. R. Rice, Localization of plastic deformation, Technical Report, Brown Univ., Providence, RI (USA). Div. of Engineering, 1976.

[14] H. B. Mühlhaus, I. Vardoulakis, The thickness of shear bands in granular materials, Géotechnique 37 (1987) 271–283.

[15] D. Houdoux, A. Amon, D. Marsan, J. Weiss, J. Crassous, Micro-slips inside a granular shear band as nano-earthquakes, arXiv preprint arXiv:2007.02867 (2020).

[16] H. Zheng, D. Wang, X. Tong, L. Li, R. P. Behringer, Granular scale responses in the shear band region, Granular Matter 21 (2019) 1–6.

[17] G. Ma, R. A. Regueiro, W. Zhou, J. Liu, Spatiotemporal analysis of strain localization in dense granular materials, Acta Geotechnica 14 (2019) 973–990.

[18] Y. Cao, J. Li, B. Kou, C. Xia, Z. Li, R. Chen, H. Xie, T. Xiao, W. Kob, L. Hong, et al., Structural and topological nature of plasticity in sheared granular materials, Nature communications 9 (2018) 1–7.

[19] A. Tordesillas, S. Pucilowski, Q. Lin, J. F. Peters, R. P. Behringer, Granular vortices: Identification, characterization and conditions for the localization of deformation, Journal of the Mechanics and Physics of Solids 90 (2016) 215 – 241.

[20] M. Oda, K. Iwashita, Study on couple stress and shear band development in granular media based on numerical simulation analyses, International journal of engineering science 38 (2000) 1713–1740.

[21] W. H. Imseeh, A. M. Druckrey, K. A. Alshibli, 3d experimental quantification of fabric and fabric evolution of sheared granular materials using synchrotron micro-computed tomography, Granular Matter 20 (2018) 24.

[22] Q. Sun, J. Zheng, Two-dimensional and three-dimensional inherent fabric in cross-anisotropic granular soils, Computers and Geotechnics 116 (2019) 103197.

[23] Z. Hu, Y. Zhang, Z. Yang, Suffusion-induced deformation and microstructural change of granular soils: a coupled cfd–dem study, Acta Geotechnica 14 (2019) 795–814.

[24] C. O'Sullivan, L. Cui, Micromechanics of granular material response during load reversals: combined dem and experimental study, Powder Technology 193 (2009) 289–302.

[25] R. J. Bathurst, L. Rothenburg, Observations on stress-force-fabric relationships in idealized granular materials, Mechanics of materials 9 (1990) 65–80.

[26] N. P. Kruyt, L. Rothenburg, Micromechanical Definition of the Strain Tensor for Granular Materials, Journal of Applied Mechanics 63 (1996) 706–711.

[27] X. Li, H.-S. Yu, On the stress–force–fabric relationship for granular materials, International Journal of Solids and Structures 50 (2013) 1285–1302.

[28] F. Nicot, F. Darve, RNVO Group: Natural Hazards and Vulnerability of Structures, A multi-scale approach to granular materials, Mechanics of Materials 37 (2005) 980 – 1006.

[29] H. Xiong, F. Nicot, Z. Y. Yin, A three-dimensional micromechanically based model, International Journal for Numerical and Analytical Methods in Geomechanics 41 (2017) 1669–1686.

[30] X. S. Shi, J. Zhao, Y. Gao, A homogenization-based state-dependent model for gap-graded granular materials with fine-dominated structure, International Journal for Numerical and Analytical Methods in Geomechanics 45 (2021) 1007–1028.

[31] G. Ma, Y. Chen, F. Yao, W. Zhou, Q. Wang, Evolution of particle size and shape towards a steady state: Insights from fdem simulations of crushable granular materials, Computers and Geotechnics 112 (2019) 147–158.

[32] J. Yang, X. Luo, The critical state friction angle of granular materials: does it depend on grading?, Acta Geotechnica 13 (2018) 535–547.

[33] H. Xiong, H. Wu, X. Bao, J. Fei, Investigating effect of particle shape on suffusion by cfd-dem modeling, Construction and Building Materials 289 (2021) 123043.

[34] J. Yang, X. Luo, Exploring the relationship between critical state and particle shape for granular materials, Journal of the Mechanics and Physics of Solids 84 (2015) 196–213.

[35] S. Zhao, T. M. Evans, X. Zhou, Shear-induced anisotropy of granular materials with rolling resistance and particle shape effects, International Journal of Solids and Structures 150 (2018) 268–281.

[36] C. Shen, S. Liu, L. Wang, Y. Wang, Micromechanical modeling of particle breakage of granular materials in the framework of thermomechanics, Acta Geotechnica 14 (2019) 939–954.

[37] Y. Zhang, G. Buscarnera, Breakage mechanics for granular materials in surface-reactive environments, Journal of the Mechanics and Physics of Solids 112 (2018) 89–108.

[38] W. Zhou, D. Wang, G. Ma, X. Cao, C. Hu, W. Wu, Discrete element modeling of particle breakage considering different fragment replacement modes, Powder Technology 360 (2020) 312–323.

[39] X. Shi, K. Liu, J. Yin, Effect of initial density, particle shape, and confining stress on the critical state behavior of weathered gap-graded granular soils, Journal of Geotechnical and Geoenvironmental Engineering 147 (2021) 04020160.

[40] J. Liu, F. Nicot, W. Zhou, Sustainability of internal structures during shear band forming in 2d granular materials, Powder Technology 338 (2018) 458 – 470.

[41] M. R. Kuhn, Structured deformation in granular materials, Mechanics of Materials 31 (1999) 407 – 429.

[42] H.-X. Zhu, Z.-Y. Yin, Grain rotation-based analysis method for shear band, Journal of Engineering Mechanics 145 (2019) 04019073.

[43] Y. Wang, Y. Wang, J. Zhang, Connecting shear localization with the long-range correlated polarized stress fields in granular materials, Nature Communications 11 (2020) 4349.

[44] J. F. Peters, M. Muthuswamy, J. Wibowo, A. Tordesillas, Characterization of force chains in granular material, Phys. Rev. E 72 (2005) 041307.

[45] A. Tordesillas, M. Muthuswamy, On the modeling of confined buckling of force chains, Journal of the Mechanics and Physics of Solids 57 (2009) 706 – 727.

[46] N. Deng, A. Wautier, Y. Thiery, Z.-Y. Yin, P.-Y. Hicher, F. Nicot, On the attraction power of critical state in granular materials, Journal of the Mechanics and Physics of Solids 149 (2021) 104300.

[47] D. Houdoux, T. B. Nguyen, A. Amon, J. Crassous, Plastic flow and localization in an amorphous material: experimental interpretation of the fluidity, Physical Review E 98 (2018) 022905.

[48] F. Darve, F. Nicot, A. Wautier, J. Liu, Slip lines versus shear bands: Two competing localization modes, Mechanics Research Communications 114 (2021) 103603. Special Issue in Honor of Prof. N. D. Cristescu.

[49] J. Liu, A. Wautier, W. Zhou, F. Nicot, F. Darve, Incremental shear strain chain: a mesoscale concept for granular plasticity, ???? Under Review.

[50] A. Wautier, S. Bonelli, F. Nicot, Scale separation between grain detachment and grain transport in granular media subjected to an internal flow, Granular Matter 19 (2017) 22.

[51] H. Zhu, F. Nicot, F. Darve, Meso-structure evolution in a 2d granular material during biaxial loading, Granular Matter 18 (2016) 3.

[52] J. Liu, A. Wautier, S. Bonelli, F. Nicot, F. Darve, Macroscopic softening in granular materials from a mesoscale perspective, International Journal of Solids and Structures 193-194 (2020) 222 – 238.

[53] V. Šmilauer, et al., Yade Documentation 2nd ed, The Yade Project, 2015. Http://yade-dem.org/doc/.

[54] A. Le Bouil, A. Amon, S. McNamara, J. Crassous, Emergence of cooperativity in plasticity of soft glassy materials, Phys. Rev. Lett. 112 (2014) 246001.

[55] M. R. Kuhn, K. Bagi, Contact rolling and deformation in granular media, International journal of solids and structures 41 (2004) 5793–5820.

[56] S. Luding, J. Duran, E. Clément, J. Rajchenbach, Simulations of dense granular flow: Dynamic arches and spin organization, Journal de Physique I 6 (1996) 823–836.

[57] S. Luding, M. Lätzel, W. Volk, S. Diebels, H. Herrmann, From discrete element simulations to a continuum model, Computer methods in applied mechanics and engineering 191 (2001) 21–28.

[58] L. Zhang, N. G. H. Nguyen, S. Lambert, F. Nicot, F. Prunier, I. Djeran-Maigre, The role of force chains in granular materials: from statics to dynamics, European Journal of Environmental and Civil Engineering 21 (2017) 874–895.

[59] D. W. Lefever, Measuring geographic concentration by means of the standard deviational ellipse, American Journal of Sociology 32 (1926) 88–94.

[60] R. Lehoucq, J. Weiss, B. Dubrulle, A. Amon, A. Le Bouil, J. Crassous, D. Amitrano, F. Graner, Analysis of image vs. position, scale and direction reveals pattern texture anisotropy, Frontiers in Physics 2 (2015).

[61] T. Stegmann, J. Toeroek, L. Brendel, D. E. Wolf, Minimal dissipation theory and shear bands in biaxial tests, GRANULAR MATTER 13 (2011) 565–572.

[62] M. Oda, H. Kazama, Microstructure of shear bands and its relation to the mechanisms of dilatancy and failure of dense granular soils, Geotechnique 48 (1998) 465–481.

[63] P. Fu, Y. F. Dafalias, Relationship between void- and contact normal-based fabric tensors for 2d idealized granular materials, International Journal of Solids and Structures 63 (2015) 68 – 81.

[64] N. Kruyt, Micromechanical study of fabric evolution in quasi-static deformation of granular materials, Mechanics of Materials 44 (2012) 120 – 129. Microstructures and Anisotropies.

[65] N.-S. Nguyen, H. Magoariec, B. Cambou, A. Danescu, Analysis of structure and strain at the meso-scale in 2d granular materials, International Journal of Solids and Structures 46 (2009) 3257 – 3271.

[66] F. Nicot, L. Sibille, F. Darve, Failure in rate-independent granular materials as a bifurcation toward a dynamic regime, International Journal of Plasticity 29 (2012) 136–154.

[67] F. Alonso-Marroquín, S. Luding, H. J. Herrmann, I. Vardoulakis, Role of anisotropy in the elastoplastic response of a polygonal packing, Phys. Rev. E 71 (2005) 051304.

[68] K. Hashiguchi, S. Tsutsumi, Gradient plasticity with the tangential-subloading surface model and the prediction of shear-band thickness of granular materials, International Journal of Plasticity 23 (2007) 767–797.

[69] A. Tordesillas, S. Pucilowski, D. M. Walker, J. F. Peters, L. E. Walizer, Micromechanics of vortices in granular media: connection to shear bands and implications for continuum modelling of failure in geomaterials, International Journal for Numerical and Analytical Methods in Geomechanics 38 (2014) 1247–1275.

[70] Z.-H. Shi, H. Horii, Microslip model of strain localization in sand deformation, Mechanics of Materials 8 (1989) 89 – 102.

[71] K. Karimi, J. L. Barrat, Correlation and shear bands in a plastically deformed granular medium, Scientific Reports 8 (2018) 4021.

[72] A. Singh, V. Magnanimo, K. Saitoh, S. Luding, Effect of cohesion on shear banding in quasistatic granular materials, Physical Review E 90 (2014) 022202.

[73] T. B. Nguyen, A. Amon, Experimental study of shear band formation: Bifurcation and localization, EPL 116 (2016).